5-2013

Study of Inkjet Printing as an Ultra-Low-Cost Antenna Prototyping Method and Its Application to Conformal Wraparound Antennas for Sounding Rocket Sub-Payload

Maimaitirebike Maimaiti
Utah State University

STUDY OF INKJET PRINTING AS AN ULTRA-LOW-COST ANTENNA PROTOTYPING METHOD AND ITS APPLICATION TO CONFORMAL WRAPAROUND ANTENNAS FOR SOUNDING ROCKET SUB-PAYLOAD

by

Maimaitirebike Maimaiti

A thesis submitted in partial fulfillment
of the requirements for the degree

of

MASTER OF SCIENCE

in

Electrical Engineering

Approved:

Dr. Reyhan Baktur Major Professor	Dr. Jacob Gunther Committee Member
Dr. Edmund Spencer Committee Member	Dr. Mark R. McLellan Vice President for Research and Dean of the School of Graduate Studies

UTAH STATE UNIVERSITY
Logan, Utah

2013

Abstract

Study of Inkjet Printing as an Ultra-Low-Cost Antenna Prototyping Method and Its Application to Conformal Wraparound Antennas for Sounding Rocket Sub-Payload

by

Maimaitirebike Maimaiti, Master of Science

Utah State University, 2013

Major Professor: Dr. Reyhan Baktur
Department: Electrical and Computer Engineering

Inkjet printing is an attractive patterning technology that has received tremendous interest as a mass fabrication method for a variety of electronic devices due to its manufacturing flexibility and low-cost feature. However, the printing facilities that are being used, especially the inkjet printer, are very expensive. This thesis introduces an extremely cost-friendly inkjet printing method using a printer that costs less than $100. In order to verify its reliability, linearly and circularly polarized (CPd) planar and conformal microstrip antennas were fabricated using this printing method, and their measurement results were compared with copper microstrip antennas. The result shows that the printed microstrip antennas have similar performances to those of the copper antennas except for lower efficiency. The effects of the conductivity and thickness of the ink layer on the antenna properties were studied, and it is found that the conductivity is the main factor affecting the radiation efficiency, though thicker ink yields more effective antennas.

This thesis also presents the detailed antenna design for a sub-payload. The sub-payload is a cylindrical structure with a diameter of six inches and a height of four inches. It has four booms coming out from the surface, which are used to measure the variations of the energy flow into the upper atmosphere in and around the aurora. The sub-payload has

two types of antennas: linearly polarized (LPd) S-band antennas and right-hand circularly polarized (RHCPd) GPS antennas. Each type of antenna has various requirements to be fully functional for specific research tasks. The thesis includes the design methods of each type of antenna, challenges that were confronted, and the possible solutions that were proposed. As a practical application, the inkjet printing method was conveniently applied in validating some of the antenna designs.

(85 pages)

Public Abstract

Study of Inkjet Printing as an Ultra-Low-Cost Antenna Prototyping Method and Its Application to Conformal Wraparound Antennas for Sounding Rocket Sub-Payload

by

Maimaitirebike Maimaiti, Master of Science

Utah State University, 2013

Major Professor: Dr. Reyhan Baktur
Department: Electrical and Computer Engineering

Inkjet printing is a type of computer printing that creates an image by propelling droplets of ink onto paper. It is an attractive patterning technology that has received tremendous interest as a mass fabrication method for a variety of electronic devices due to its manufacturing flexibility and low-cost feature. However, the printing facilities that are being used, especially the inkjet printer, are very expensive. This thesis introduces an extremely cost-friendly inkjet printing method using a printer that costs less than $100. In order to verify its reliability, linearly and circularly polarized planar and conformal microstrip antennas were fabricated using the printing method, and their measurement results were compared with copper microstrip antennas. The result shows that the printed microstrip antennas have similar performances to those of the copper antennas except for lower efficiency. The effects of the conductivity and thickness of the ink layer on the antenna properties were studied, and it is found that the conductivity is the main factor affecting the radiation efficiency, though thicker ink yields more effective antennas.

This thesis also presents the detailed antenna design for a sub-payload. The sub-payload is a cylindrical structure with a diameter of six inches and a height of four inches. It has four booms coming out from the surface, which are used to carry out scientific

measurement in the North Pole atmosphere. The sub-payload has two types of antennas: linearly polarized (LPd) S-band antennas and right-hand circularly polarized (RHCPd) GPS antennas. Each type of antenna has various requirements to be fully functional for specific research tasks. The thesis includes the design methods of each type of antenna, challenges that were confronted, and the possible solutions that were proposed. As a practical application, the inkjet printing method was conveniently applied in validating some of the antenna designs.

Acknowledgments

First, I would like to express my deep gratitude to my advisor, Dr. Reyhan Baktur, for her patient guidance, enthusiastic encouragement, and valuable and constructive suggestions during the planning and development of this research work. Her willingness to give her time so generously has been very much appreciated. I would also like to thank the other members of my supervisory committee, Dr. Jacob Gunther and Dr. Edmund Spencer, for giving me the necessary support needed for the successful completion of my work.

I would like to thank Dr. Charles Swenson and Chadwin Fish of the Space Dynamics Laboratory for entrusting me with the sub-payload antenna design project and providing me with valuable insight. I also thank Weston Nelson of the Space Dynamics Laboratory for helping me fabricate the cylindrical sub-payload model needed in carrying out my research. I would also like to give my special thanks to the staff of the Electrical Engineering Department at Utah State University for providing me all the necessary help whenever needed. Special thanks to Mary Lee Anderson for her kind help on several occasions.

My profound gratitude also goes to Tusunjan Yasin for his readiness to provide valuable insight and generous help throughout my research. I also thank the other members of my research group for their assistance: Olutosin C. Fawole, Jesus A. Arellano, Taha Shahvirdi, and Salahuddin Tariq.

Finally, I would like to thank all of my friends who have supported me socially and emotionally throughout my stay in Logan. My days in Logan were brightened because of them.

Maimaitirebike Maimaiti

Contents

List of Tables

List of Figures

Acronyms

ADS	advanced design system
AR	axial ratio
ASSP	auroral spatial structures probe
CAD	computer-aided design
CMYK	cyan, magenta, yellow, black
CP	circular polarization
CPd	circularly polarized
HFSS	high frequency structural simulator
LP	linear polarization
LPd	linearly polarized
NSI	Nearfield Systems Inc.
OEM	original equipment manufacturer
RFID	radio-frequency identification
RHCPd	right-hand circularly polarized
VSWR	voltage standing wave ratio

Chapter 1

Introduction

Inkjet printing is a type of computer printing that creates a digital image by propelling droplets of ink onto a printing substrate. The operating principle of inkjet printing process can be briefly explained as follows.

The chambers (cartridges) of an inkjet house a piezoelectric material and are connected to nozzles. When the voltage is applied, the piezoelectric actuator changes its volume. As a result, a pressure wave is formed and begins propagating throughout the capillary. When a positive pressure wave approaches the nozzle, ink droplets are pushed outward towards the printing substrate [1].

Inkjet printing has a number of attributes that make it a hot research topic in microwave circuit fabrication. These include simplicity, compatibility with a variety of substrates, direct complex pattern printing from computer-aided design (CAD) files, low-cost, non-contact, and high-speed parallel nozzle printing [2, 3]. Due to the above mentioned features, inkjet printing could be a better alternative to the circuit board fabrication and photolithography widely used in actual industrial manufacturing.

It is reported that, using inkjet printing method, the electronic devices can be printed on papers, surface treated glasses, photo papers, and other specially coated polyethylene terephthalate (PET) films. For example, inkjet printing has been used in printing coplanar waveguides transmission lines on surface-treated glasses [4], passive devices suitable for a radio-frequency identification (RFID) front-end on plastic substrates [5], and multilayer patch resonator band pass filter, RFID tags, and ultra wideband antennas on commercially available paper sheets [6–8]. Although inkjet printing itself is very cost-friendly, the inkjet printing facilities, especially the inkjet printers, that have been used are usually very expensive as is the case in the above applications where Dimatix printers are chosen. Although

these printers are quite precise, a lot of labs cannot afford the price. Also, there are many cases where the engineers want to verify their design quickly at low-cost, though with less precise methods, before they go into the actual fabrication of the devices in order to avoid possible waste of effort and materials. Therefore, there is a need to lower the cost of inkjet printing.

Motivated by the necessity of lowering the cost of inkjet printing, this thesis introduces an extremely cost-friendly inkjet printing method which requires a printer worth less than $100. The printing facilities also include conductive ink, transparency, cleaning solution, and an oven. The printing process can be briefly explained as follows.

The pattern of an antenna or any other device, after a "print" command is given to the inkjet printer, is printed on the transparency using the conductive ink. The printed pattern is then cured in an oven. After printing, the cleaning solution is used for cleaning the printer's head and for maintaining the normal performance of the printer. The detailed printing method is presented in Chapter 2.

This printing method was first introduced by Jesus Arellano, but it was not mature enough to be used in prototyping antennas with reliable performance. This research work has improved his printing method, and its reliability has been verified by prototyping and measuring various types of microstrip patch antennas. The second phase of the research is an antenna design project for a cylindrical sub-payload, which involves designing, prototyping, and testing LPd conformal S-band and CPd conformal L-band patch antennas. This is also a practical application of the inkjet printing method as it has been conveniently applied in validating some of the antenna designs.

This thesis is organized into four chapters. Chapter 1 introduces the research presented in this thesis. Chapter 2 presents the inkjet printing method that has been developed. In this chapter, the inkjet printing facilities and printing procedures are explained in detail. The fast and cost-friendly features of the printing method are demonstrated by prototyping LPd and CPd planar and conformal microstrip antennas. Performance evaluation is carried out by comparing the measurement results of the printed antennas with copper antennas.

It is observed that the printed antennas have lower radiation efficiency than the copper antennas. The cause of the low efficiency is addressed, and a good simulation model for the printed patch antenna is also provided. Chapter 3 details the antenna design process for the sub-payload. In this chapter, the design of LPd conformal S-band patch antenna array and CPd L-band patch antenna array are explained in detail, challenges are addressed, and possible solutions are proposed. Chapter 4 summarizes this work and highlights the future work that could be done.

Chapter 2

Ultra Low-Cost InkJet Printing Method

2.1 Printing Method

This work of inkjet printed patch antennas is a continuation of a previous thesis research of Jesus Arellano [9]. The printing procedures have been explained in detail in that thesis. The current work aims to improve Arellano's printing method to yield a more efficient and reliable antenna prototyping technique. For the ease of reading and understanding the printing routine, some procedures from Arellano's work are repeated here.

The inkjet printing facilities at USU consist of an Epson printer, conductive ink, transparency, and Metalon aqueous vehicle. The Epson printer is shown in Fig. 2.1, which costs less than $100. This printer uses the advantageous CMYK (Cyan, Magenta, Yellow, Black) drop-on-demand Micro Piezo inkjet technology. An antenna is printed on the transparency – Novele^{TM} coated polyethylene terephthalate (PET) film – using Nanosilver aqueous dispersive ink Metalon JS-B25P from Novacentrix (Fig. 2.2). The PET film is specifically engineered to hold Metalon conductive inks. The Metalon aqueous vehicle is a cleaning solution necessary for cleaning the printer's head after its use and for maintaining the normal performance of the printer. After printing the antenna, a curing process is performed to evaporate the solvent present in the conductive ink. The following is a detailed introduction to the whole printing process.

2.1.1 Pre-Printing Routine

After a successful connection between the Epson printer and a personal computer, the Epson original equipment manufacturer (OEM) cartridges are installed in their due positions in the printer in order for the printer to be initialized. After that, the nozzle condition must be checked to assure that the printer nozzle is free from clogging. If the

Fig. 2.1: Epson Stylus® C88+, <= $100.00.

Fig. 2.2: Conductive ink from Novacentrix.

nozzle check is faulty, then head cleaning is required. The faulty nozzle can be identified by comparing the printed nozzle check pattern with the standard one shown on the computer. The nozzle check and head cleaning process need to be repeated until the nozzle check pattern is satisfactory. Following the nozzle check, the empty refillable CMYK cartridges are filled with the Metalon aqueous vehicle cleaning solution, which is used to clean the nozzle from the traces of ink. These cartridges should go through a priming process before use. To do this, a 10 mL slip tip syringe is inserted through the exit port of the cartridge while gently suctioning the vehicle through the cartridge until liquid enters the syringe. At this point, it is important to first remove both rubber stoppers from the filling ports (Fig. 2.3), otherwise no liquid will be suctioned. It is also useful to try to wet the bottom of the cartridges with the help of metal needle. After that, the OEM cartridges are replaced with the refillable cartridges filled with Metalon aqueous vehicle cleaning solution, and large block patterns with yellow, cyan, magenta, black colors are printed. It is important that the block pictures must be printed with the setting “black ink only” option selected in the print panel. This helps wash out the traces of the original ink and prepares the printer for the conductive ink. Printing the block pictures should be continued until no traces of the original inks are seen on the paper.

Fig. 2.3: Cartridge priming.

2.1.2 Printing Routine

After the nozzle has been cleaned, only the black refillable cartridge filled with the Metalon aqueous vehicle cleaning solution is replaced with the black refillable cartridge filled with the Metalon JS-B525P conductive ink. The filling and priming processes of the refillable cartridge for the Metolon conductive ink are the same as those of the refillable cartridge for the Metalon aqueous vehicle. After the installation of the black refillable cartridge filled with conductive ink, the nozzle check is performed again to see if the conductive ink can smoothly come out from the nozzle. If the nozzle check is faulty, the head cleaning should be done repeatedly. Usually, if the traces of the original ink are washed well, the nozzle check result will be satisfactory. Following the nozzle check, the PET film is placed to print the designed antenna pattern exported from the HFSS to the AutoCAD. To get the best results, the following should be set from the "Advanced Printing" option: choose the Quality Option as "Best Photo," the Paper Type as "Matte-Paper-Heavyweight," and check "Grayscale," uncheck "High Speed" in the Print Options.

The above printing method is almost the same as that introduced in Arellano's thesis. Although the above printing process gives the best printing result it can possibly offer, the printed patch is actually a combination of many parallel lines with tiny gaps between them and is semi-transparent. This is due to the resolution of the printer that is used.

Apparently, the gaps need to be filled to make the printed antenna solid. One way of doing that is the touch-up method, which was used by Jesus, where the printed antenna is painted with the conductive ink using a fine brush. This requires a great care and is time consuming. Besides, it is impossible to guarantee that the painting falls within the antenna frame and that the conductive ink is uniformly distributed on the PET film. Another way of solving the problem is to print the antenna pattern multiple times, which is the main improvement introduced to Jesus' printing method. Due to the tiny vibrations of the printer during the printing process, the gaps can be covered by reprinting the same pattern several times. This should be done before curing, and there should be approximately a one-minute interval between each two prints. Also, it is necessary to load the PET film against the right edge guide and slide the left edge guide to a position such that there is barely enough space for the PET film to pass through. In this way, the antennas printed each time almost overlap each other. Usually, printing three to five times gives a good, solid printed antenna. Printing multiple times is the key to make the printed antenna solid enough to perform as a good antenna. Figure 2.4 shows the printed antenna without using the introduced inkjet printing method. Figures 2.5-2.6 are the antennas printed once and multiple times, respectively, using the inkjet printing method. Figures 2.7-2.8 are the building blocks of array antennas printed multiple times. It can be seen that the inkjet printing method, when applied multiple times, significantly improves the quality of the printed antennas.

2.1.3 Post-Printing Routine

After printing the antenna, it is essential to cure the prototype in order to increase the conductivity of the conductive ink. This can be done through air drying or baking in an oven. Baking is a better curing option than air drying since it gives more uniform ink distribution on the PET film, yields better conductivity values, and is faster. Baking can be done in an oven (Fig. 2.9) under the temperature of 100-110 Celsius for three to four hours.

Although the printing method is introduced in three steps, the first step can be skipped if the printer has been regularly used for the inkjet printing. Also, if it is certain that the

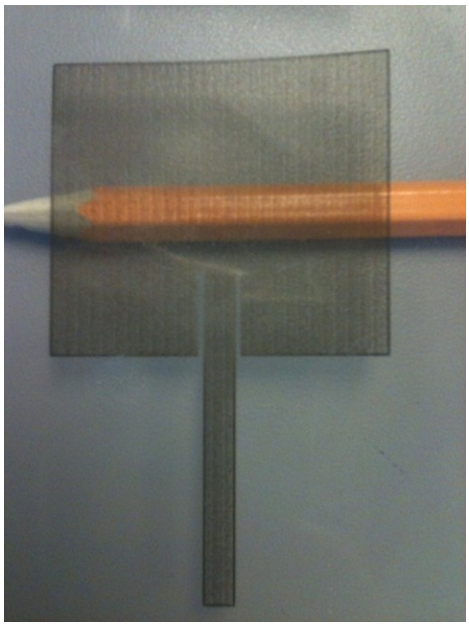

Fig. 2.4: Patch antenna printed once without using the printing method.

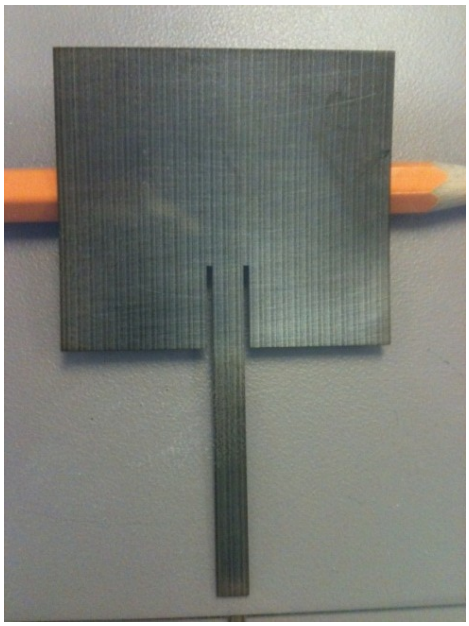

Fig. 2.5: Patch antenna printed once using the printing method.

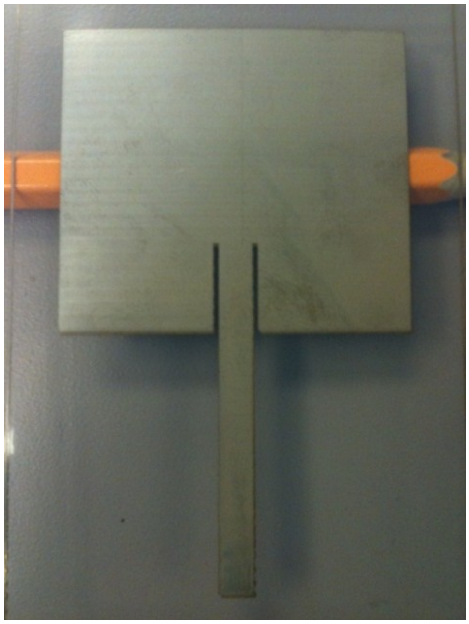

Fig. 2.6: Patch antenna printed multiple times using the printing method.

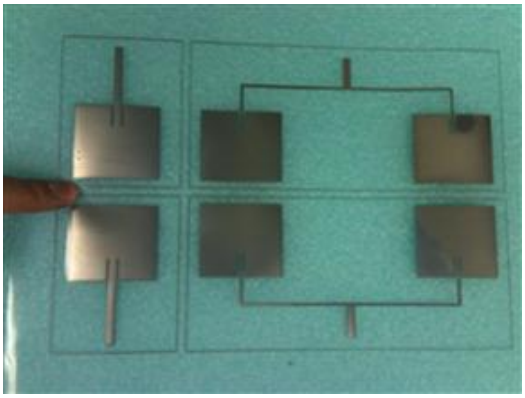

Fig. 2.7: Patch antenna printed multiple times (front side).

Fig. 2.8: Patch antenna printed multiple times (back side).

printer will not be used for more than a week, then after finishing the printing, the printer should be cleaned using the Metalon aqueous vehicle cleaning solution by printing block patters in the same way mentioned in the pre-printing routine.

The thickness of the printed antenna varies depending on printer settings, age of the printer, etc. but typically the print will be about 500-1000 nm. However, the cured print is still porous (around 50%). If 500 nm is taken as the thickness of one layer of conductive ink on PET, printing five times gives a printed pattern with a 2.5 µm of ink thickness.

2.2 InkJet Printed Patch Antenna - Prototyping and Measurement

In order to demonstrate the reliability of the inkjet printing method, LPd and CPd S-band patch antennas, both in planar and conformal cases, were fabricated and tested in an anechoic chamber with NSI near-field systems. The following sections present the work in detail.

2.2.1 Linearly Polarized Planar Patch Antenna

A single S-band patch antenna was designed in a high frequency structural simulator (HFSS) at a center frequency of 2.225 GHZ. Its length and width are, respectively, 38.7 mm and 43.5 mm, and the inset feed recessed distance is 14.5 mm. Two antennas were fabricated, one with copper tape (Fig. 2.10) and the other with conductive ink using the inkjet printing method (Fig. 2.11). For inkjet printed antenna prototyping, the HFSS design was exported into the AutoCAD and then printed on the PET film. The PET film was then cut, placed on the substrate, and stabilized with scotch tape as shown in Fig. 2.11. It should be noted that the polycarbonate was used as the antenna substrate since its cost is low and it is easy to be wrapped around a cylindrical structure. The thickness of the substrate is 1.524 mm and the permittivity is 2.9. The measured directivity, gain, and efficiency of the copper antenna are 7.831 dB, 4.295 dB, and 44.3%, respectively; and the measured directivity, gain, and efficiency of the printed antenna are, respectively, 8.205 dB, 4.468 dB, and 42.3%. The efficiency of the copper antenna is higher than that of the inkjet antenna due to the lower conductivity of the ink. The measured S11 and radiation patterns

Fig. 2.9: Oven for curing the printed antennas.

are shown in Figs. 2.12-2.17. Compared to the copper antenna, the printed antenna has a greater frequency shift, which is due to the fact that the PET film and the scotch tape were not modeled in HFSS. Also, in the planar case, it is hard to completely squeeze out the air between the patch and the substrate when taping the printed antenna on the substrate. However, the radiation patterns of both copper and printed antennas are almost identical.

2.2.2 Linearly Polarized Conformal Patch Antenna

Single Conformal S-Band Patch Antenna

The conformal patch antenna design is almost the same as the planar patch antenna design except that it is needed to adjust the length of the antenna in order to compensate for the bending effect [10]. Accordingly, a single conformal S-band antenna was designed in HFSS based on the dimension of the previous single planar S-band patch antenna. Its length, width, and inset feed recessed distance are 38.5 mm, 43.5 mm, and 14.5 mm, respectively. The cylinder is six inches in diameter and four inches in height. Again, two antennas were fabricated, one with copper tape (Fig. 2.18) and the other with conductive ink using the inkjet printing method (Fig. 2.19). The copper antenna's measured directivity, gain, and efficiency are 7.569 dB, 6.489 dB, and 77.97%, respectively; and the printed antenna's measured directivity, gain, and efficiency are 7.316 dB, 5.393 dB, and 64.23%, respectively.

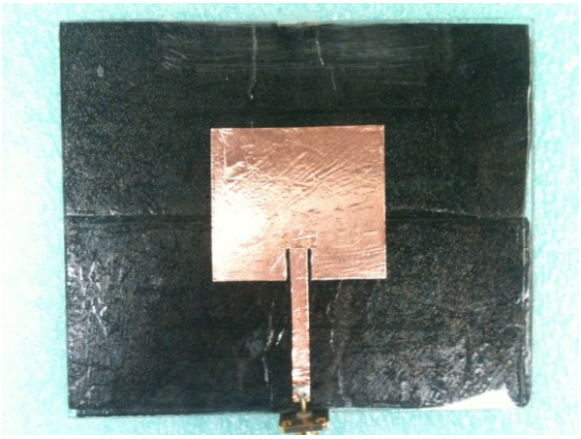

Fig. 2.10: Planar copper antenna.

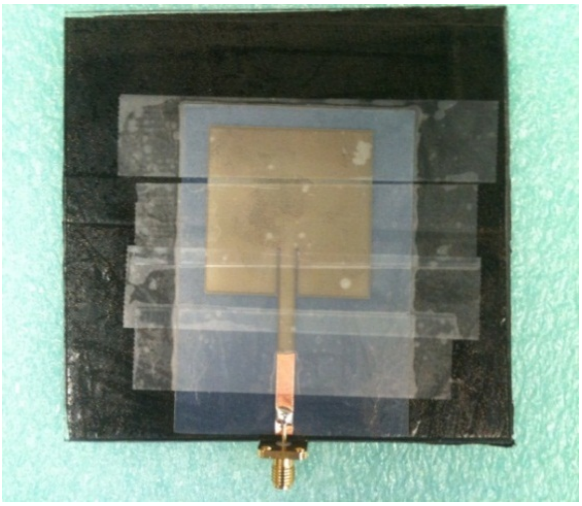

Fig. 2.11: Printed antenna.

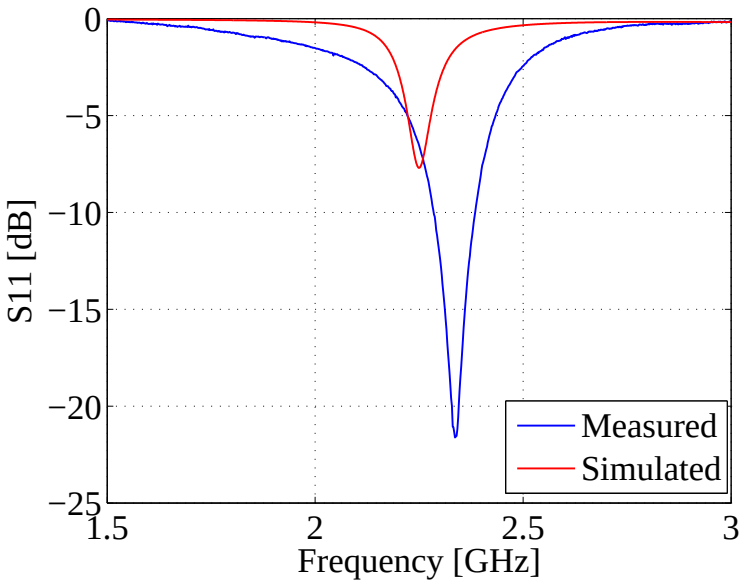

Fig. 2.12: S11 of the copper antenna.

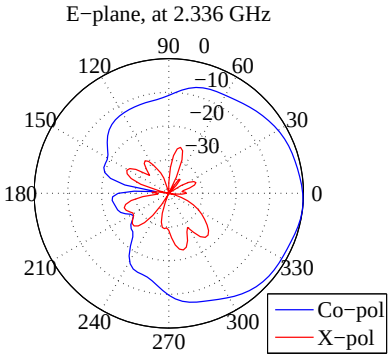

Fig. 2.13: E-plane radiation pattern of the copper antenna.

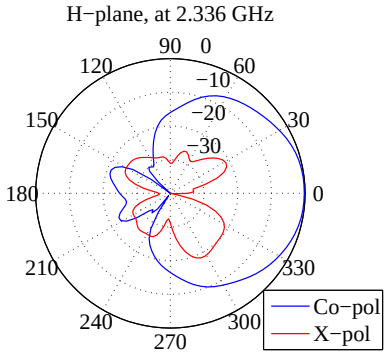

Fig. 2.14: H-plane radiation pattern of the copper antenna.

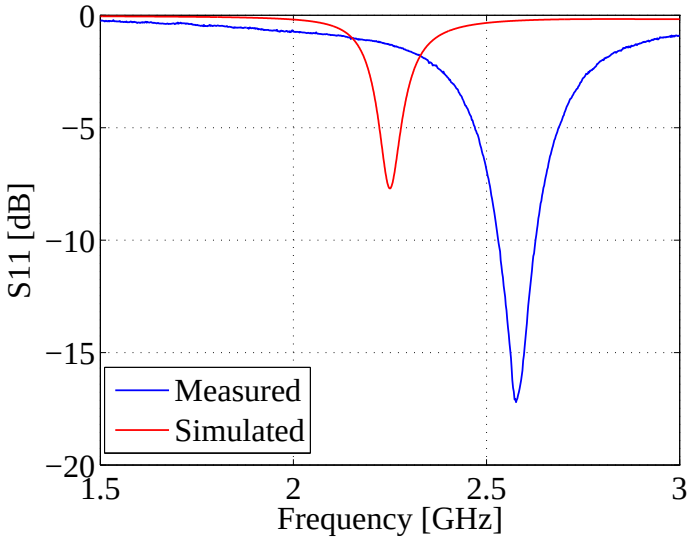

Fig. 2.15: S11 of the printed antenna.

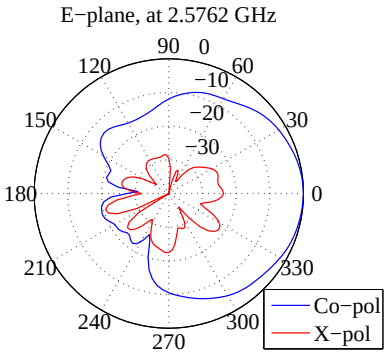

Fig. 2.16: E-plane radiation pattern of the printed antenna.

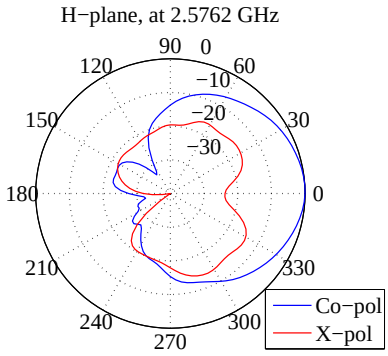

Fig. 2.17: H-plane radiation pattern of the printed antenna.

The conformal copper antenna has higher efficiency than that of the inkjet antenna due to the lower conductivity of the ink. The measured S11 parameter and radiation patterns are shown in Figs. 2.20-2.25. It can be seen that both the conformal copper antenna and the printed antenna have almost the same resonant frequencies and are very close to the simulation. This is because, in the cylindrical case, it is possible to attach the PET film very tightly to the cylindrical surface as the PET film is curved after curing in the oven. The radiation patterns of both copper and printed antennas are also the same.

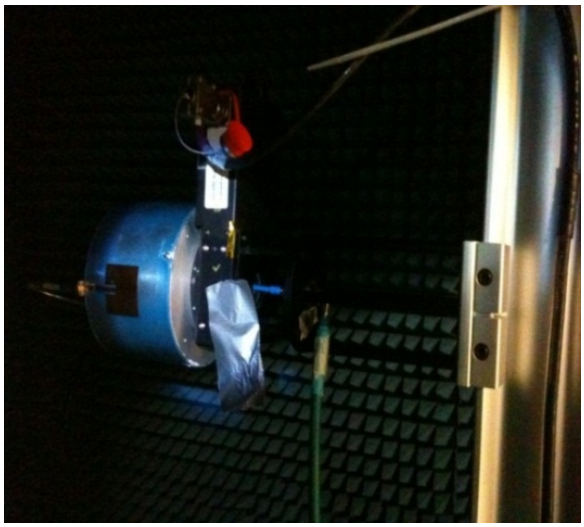

Fig. 2.18: Conformal copper antenna.

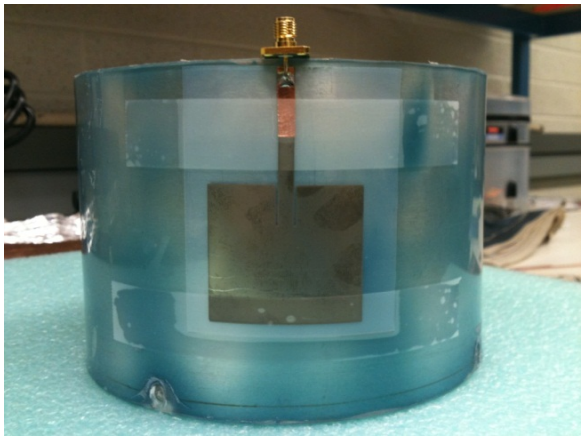

Fig. 2.19: Conformal printed antenna.

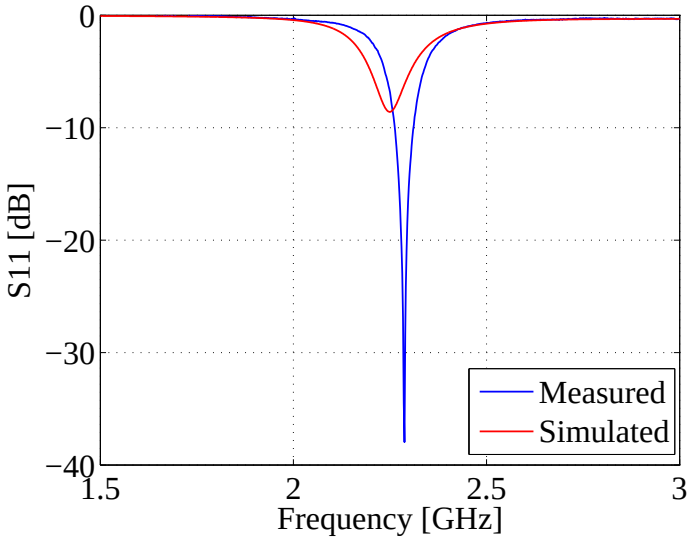

Fig. 2.20: S11 of the copper antenna.

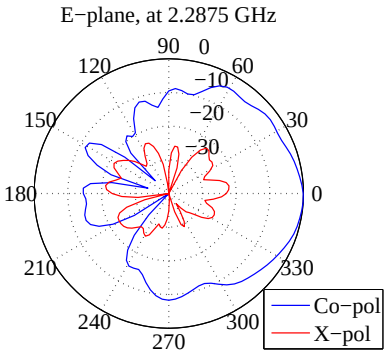

Fig. 2.21: E-plane radiation pattern of the copper antenna.

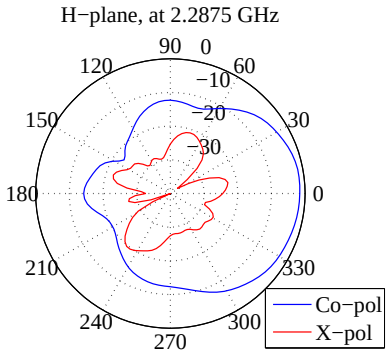

Fig. 2.22: H-plane radiation pattern of the copper antenna.

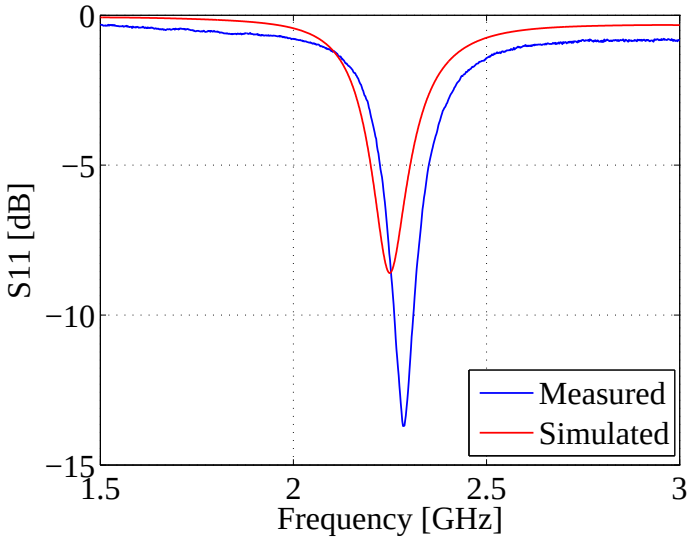

Fig. 2.23: S11 of the printed antenna.

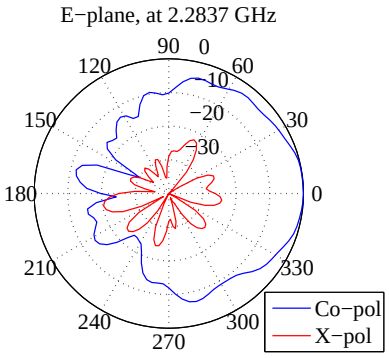

Fig. 2.24: E-plane radiation pattern of the printed antenna.

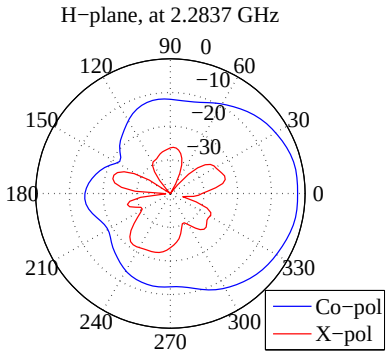

Fig. 2.25: H-plane radiation pattern of the printed antenna.

Two-Element Conformal S-Band Patch Antennas

As a simple demonstration of the inkjet printing method in prototyping patch antenna array, a two-element conformal array was designed in HFSS at a center frequency of 2.225 GHz with dimensions of 38.3 mm (width) x 43.5 mm (length) and inset feed recessed distance of 11 mm. The feed line was designed starting with a 50 Ω microstrip line with a thickness of 3.88 mm, and it was then divided into two 100 Ω microstrip lines with the same thickness of 1.045 mm. The printed two-element patch array is shown in Fig. 2.26. Its measured directivity, gain, and efficiency are 6.1 dB, 4.107 dB, and 63.2%, respectively. The simulated and measured S11 parameters and radiation patterns are shown in Figs. 2.27-2.29, where it can be observed that the measured S11 and radiation pattern agree well with the simulation results. The frequency shift is due to the PET film and the scotch tape, which were not included in the HFSS simulation. Also, there could have been some air between the patch and the substrate when taping the antenna on the substrate. These measurement results show that this type of printing method can be extended to the array-level prototyping.

2.2.3 T-Coupled Circularly Polarized Patch Antenna

Circular polarization (CP) is preferred in many applications, especially in satellite communication, as it has the advantage of greater flexibility in orientation angle between transmitter and receiver and reduction in multipath reflections [11]. Most commonly used CPd patch antennas are corner-truncated square patch antenna, nearly square diagonal-fed patch antenna and square patch antenna with a diagonal slot. There are various kinds of feeding methods, but microstrip line, coaxial probe, aperture coupling, and proximity coupling are the most common methods for exciting patch antennas [12]. For the inkjet printing, a microstrip line fed patch antenna has been chosen as the microstrip line stays on the same surface with the patch and therefore can be printed together easily.

Single T-Coupled Circularly Polarized Planar S-Band Patch Antenna

Figure 2.30 shows the geometry of the CPd patch antenna, specially designed for the demonstration of the inkjet printing method. Such a design is straightforward, where trim-

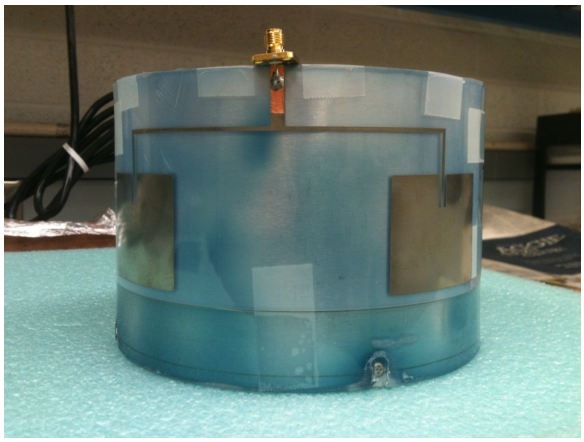

Fig. 2.26: Two-element printed antenna.

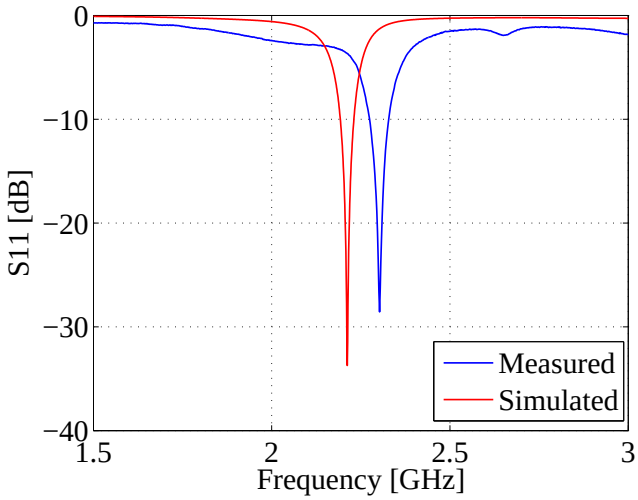

Fig. 2.27: S11 of the two-element printed antenna.

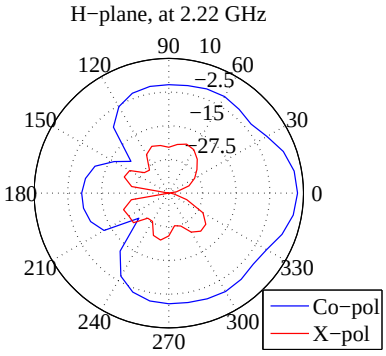

Fig. 2.28: Simulated H-plane radiation pattern of the two-element printed antenna.

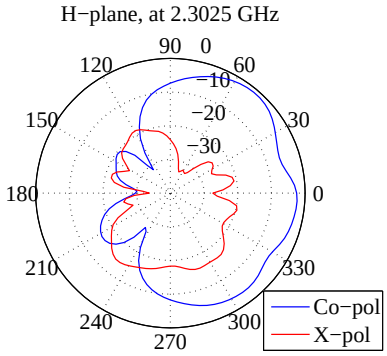

Fig. 2.29: Measured H-plane radiation pattern of the two-element printed antenna.

ming the two corners results in two orthogonal modes with 90° of phase shift [13]. The excitation happens via the coupling from the T-line. The gap (g) and the T-line width (t) are the parameters that control the impedance matching.

The T-coupled CPd patch antenna geometry was first validated through a HFSS design. The simulated parameters of the patch antenna are listed in Table 2.1. In order to verify the feasibility of such an antenna design, it was first fabricated using a circuit board milling machine. The fabricated T-coupled patch antenna is shown in Fig. 2.31. Its measured directivity, gain, and efficiency are 7.082 dB, 2.092 dB, and 31.69%, respectively. The simulated and measured S11, radiation patterns, and Axial Ratio (AR) plots are shown in Figs. 2.32-2.36. It can be seen that the measurement agrees well with the simulation, which validates the feasibility of the T-coupled CPd patch antenna design.

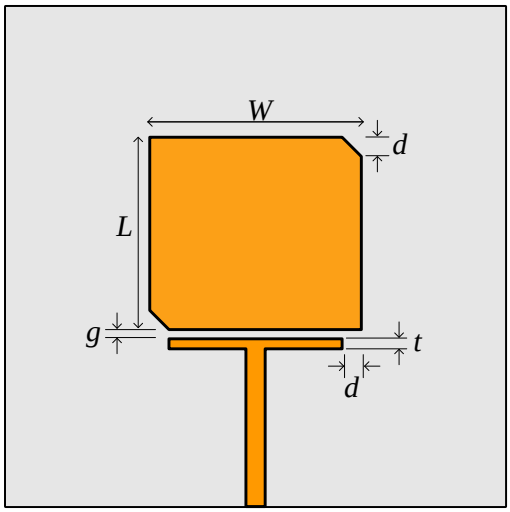

Fig. 2.30: CPd planar antenna geometry.

Table 2.1: Simulated parameters of the T-coupled CPd planar antenna.

Width (W)	34.68 mm
Length (L)	34.68 mm
Gap between the T-Line and the Antenna (g)	0.3 mm
Amount of truncation (d)	3 mm
T-line thickness (t)	1 mm

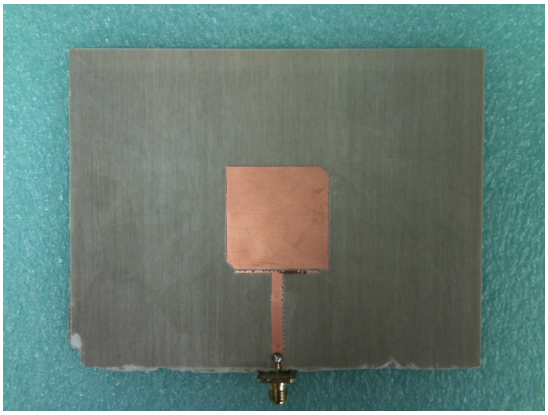

Fig. 2.31: CPd planar copper antenna.

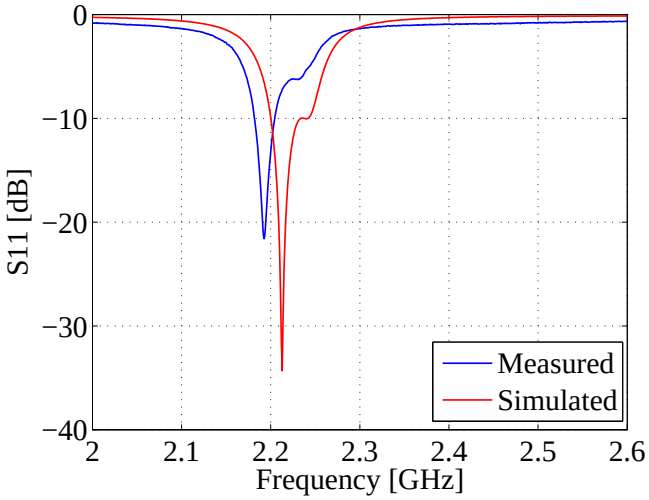

Fig. 2.32: S11 of the T-coupled CPd copper antenna.

Two-Element T-Coupled Circularly Polarized Planar S-Band Patch Antenna

In order to demonstrate that this type of antenna configuration can be expanded to the array level, a two-element T-coupled CPd patch antenna array was designed in HFSS at a center frequency of 2.225 GHz. The antenna was again fabricated using the circuit board milling machine as shown in Fig. 2.37. Its measured directivity, gain, and efficiency are 10.745 dB, 5.425 dB, and 29.38%, respectively. Figures 2.38-2.42 show the simulated and measured S11, radiation patterns, and AR plots. It is seen that the measurement agrees well with the simulation.

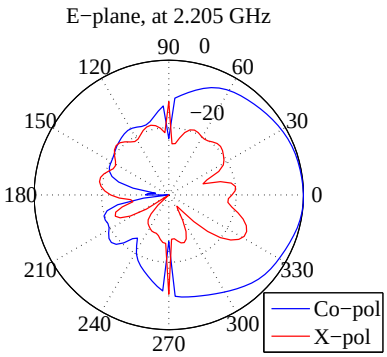

Fig. 2.33: Measured E-plane radiation pattern of the copper antenna.

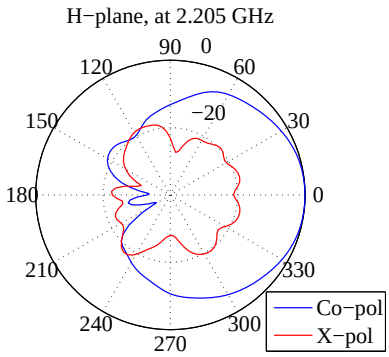

Fig. 2.34: Measured H-plane radiation pattern of the copper antenna.

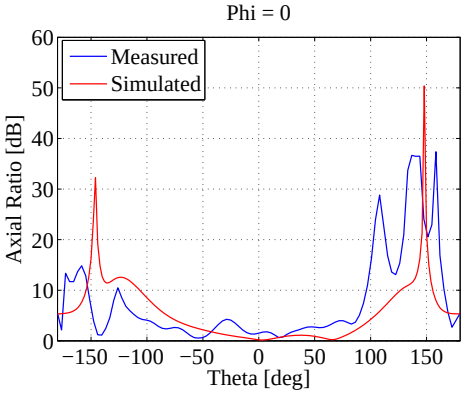

Fig. 2.35: Axial ratio at phi=0.

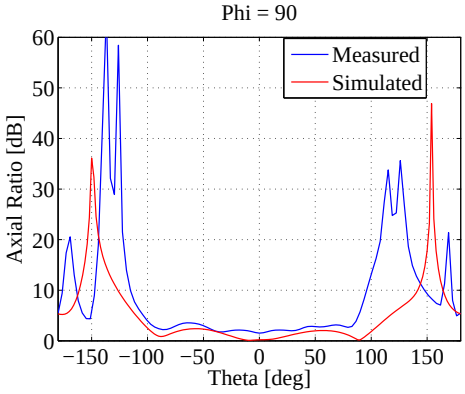

Fig. 2.36: Axial ratio at phi=90.

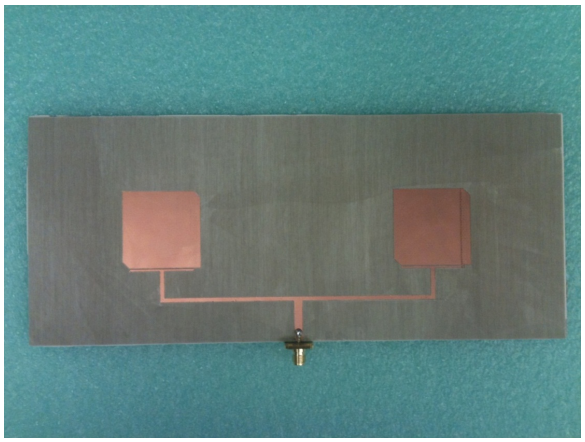

Fig. 2.37: Two-element T-coupled CPd planar copper antenna.

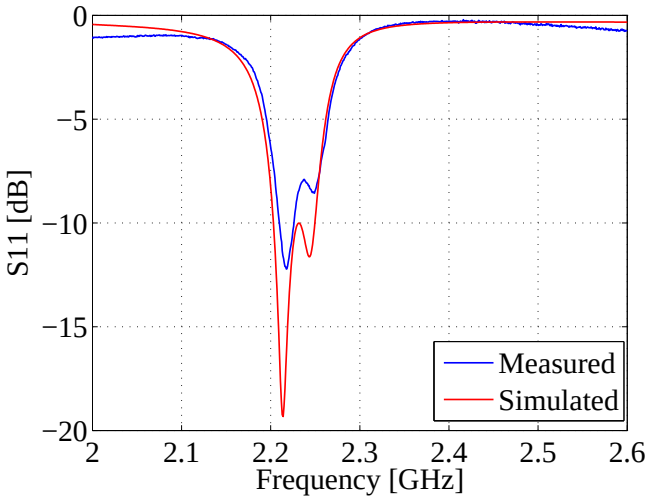

Fig. 2.38: S11 of the two-element T-coupled CPd copper antenna.

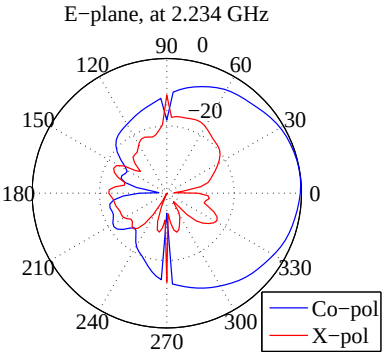

Fig. 2.39: E-plane radiation pattern of the two-element copper antenna.

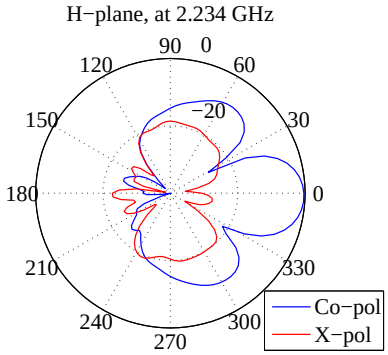

Fig. 2.40: H-plane radiation pattern of the two-element copper antenna.

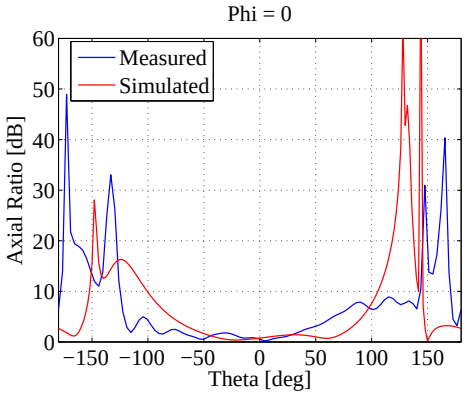

Fig. 2.41: Axial ratio at phi=0.

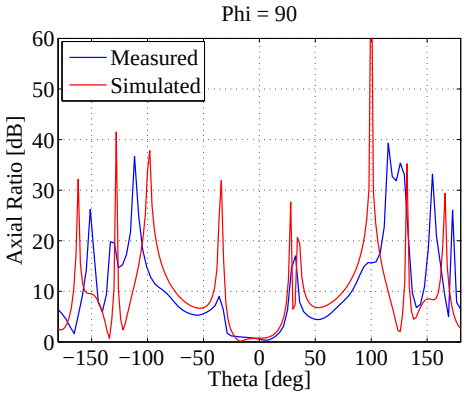

Fig. 2.42: Axial ratio at phi=90.

However, the CP property of this type of T-coupled antenna could not be achieved through the inkjet printing in planar case. This is due to the very narrow bandwidth and sensitive nature of CPd patch antenna [12]. To obtain the desired simulation results, the fabricated antenna should be as close as possible to the simulated antenna. This is the case when circuit board milling machine is used for the T-coupled CPd patch antenna fabrication since the fabricated antenna dimensions can be close enough to the simulation within acceptable tolerance. However, the printed antenna's dimensions are changed because of the multiple printing, especially the gap (g), T-line width (t), and the truncated length (d). Besides, the PET film and scotch tapes has not been included in the simulation, which is not negligible when CP property is desired. In addition, the air between the PET film and the antenna substrate is difficult to be squeezed out in the planar case.

T-Coupled Circularly Polarized Conformal S-Band Patch Antenna

Conformal CPd antenna is preferred for devices which require the antennas to be mounted on their non-planar surfaces, as is the case in the sub-payload antenna design. It is known that when bending a CPd planar antenna onto a cylindrical surface, the CP property is easily lost [14]. The CP degradation and frequency shifting were observed during the HFSS design of the T-coupled CPd conformal patch antenna (Fig. 2.43) when the parameters of the planar patch antenna were used. In order to compensate the bending effect, the length (L), gap (g), and truncated length (d) were adjusted. Table 2.2 lists the simulated parameters of the CPd conformal patch antenna.

Due to the flexible nature of the PET film, the inkjet printing method best suits in prototyping the T-coupled conformal antenna. Besides, it is possible to attach the PET film very tightly to the cylindrical surface with little air in between. Figure 2.44 shows the T-coupled CPd conformal antenna fabricated using the inkjet printing method. The simulated and measured S11, radiation patterns, and AR plots are shown in Figs. 2.45-2.51. There is a slight frequency shift, which is due to the fact that the PET film and the scotch tape were not modeled in HFSS. Also, there could have been a very small amount of air between the patch and the substrate. From Fig. 2.44, it is seen that there is a slit cut on the

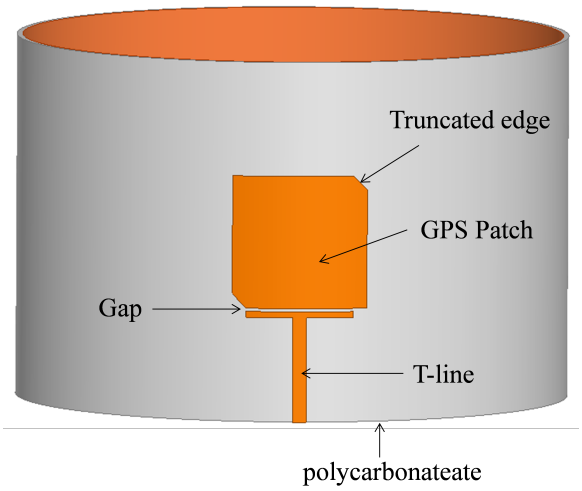

Fig. 2.43: CPd conformal antenna geometry.

Table 2.2: Simulated parameters of the T-coupled CPd conformal antenna.

Width (W)	38.38 mm
Length (L)	37.38 mm
Gap between the T-Line and the Antenna (g)	0.2 mm
Amount of truncation (d)	4 mm
T-line thickness (t)	1 mm

printed patch antenna. Such a slit was not in the design, and it was cut during the tuning for impedance matching. Because the antenna was printed multiple times to have a thicker ink layer, the gap between the T-line and the patch was inevitably affected. Therefore, the impedance matching in the prototype is no longer the same as in simulation. The slit was cut to offset the effect of the changes in the feed-line. In all, the measured radiation patterns and AR are also reasonable and agree well with the simulated results.

2.3 Effect of Conductivity and the Skin Depth

The above demonstrations show that, in terms of radiation pattern, an inkjet printed antenna has the same performance as its counterpart – copper antenna, but the efficiency of the inkjet printed antenna is lower than the copper antenna. This can be explained as follows by analyzing the effect of the conductivity and thickness of the conductive ink.

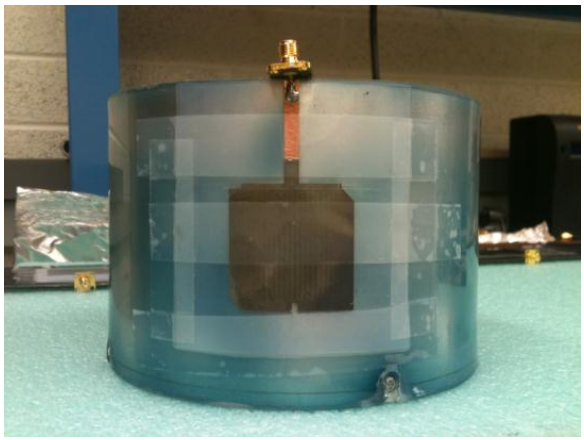

Fig. 2.44: CPd conformal printed antenna.

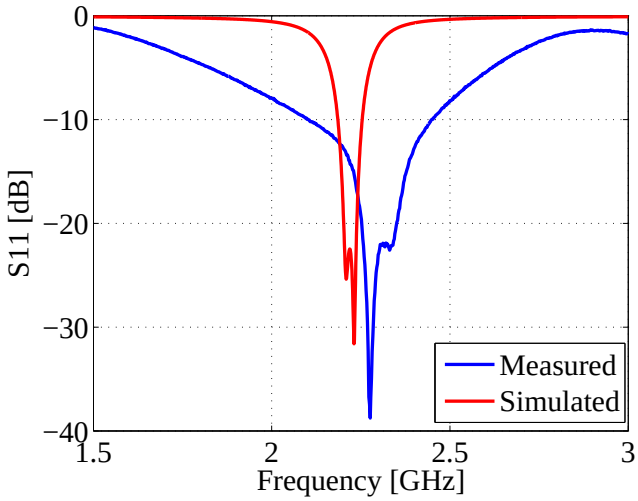

Fig. 2.45: S11 of the T-coupled CPd conformal printed antenna.

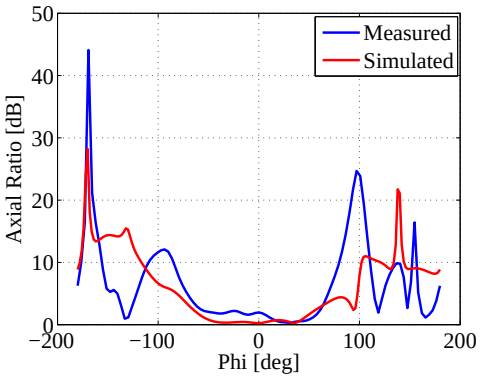

Fig. 2.46: Axial ratio of the CPd conformal printed antenna at theta=90.

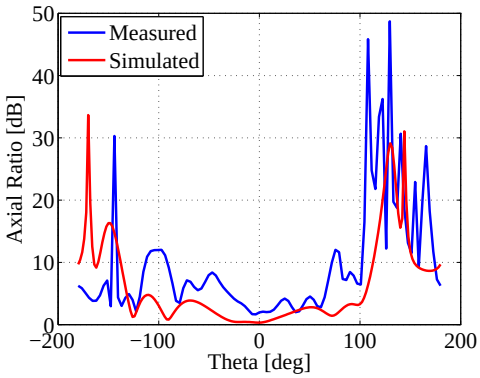

Fig. 2.47: Axial ratio of the CPd conformal printed antenna at phi=0.

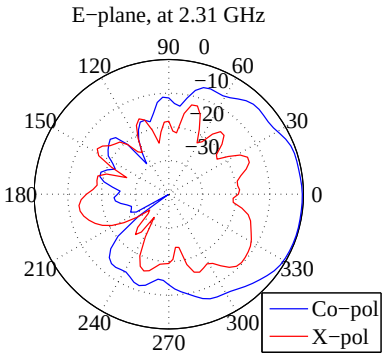

Fig. 2.48: Measured E-plane radiation pattern of the CPd conformal printed antenna.

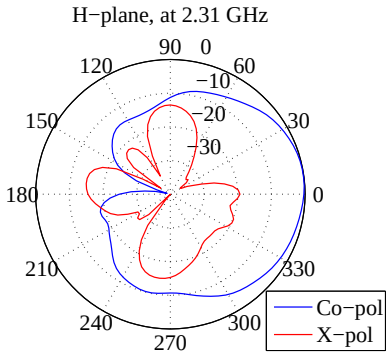

Fig. 2.49: Measured H-plane radiation pattern of the CPd conformal printed antenna.

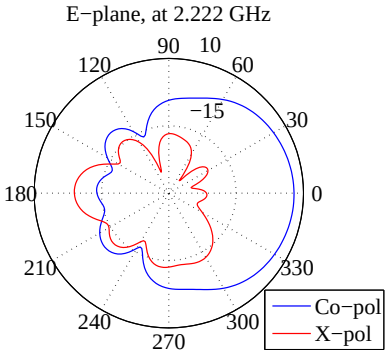

Fig. 2.50: Simulated E-plane radiation pattern of the CPd conformal printed antenna.

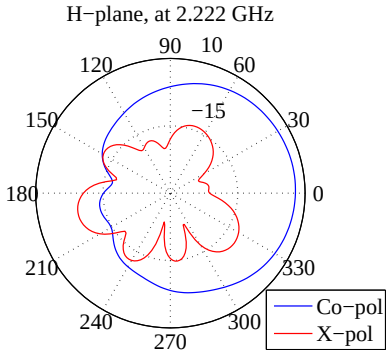

Fig. 2.51: Simulated H-plane radiation pattern of the CPd conformal printed antenna

It is well understood that the thickness of a radiating metal should be larger than the skin depth, which can be computed from Eq. (2.1)

$$\delta_s = \sqrt{\frac{1}{\pi f \mu_o \sigma}}, \tag{2.1}$$

where δ_s is the skin depth, f is the frequency, μ_o is the free space permeability, and σ is the conductivity. An antenna pattern printed multiple times, after curing, can be considered as a good conductor but not as good as a copper sheet. Therefore, the conductivity of the ink is represented as

$$\sigma = \sigma_c k_{def}, \tag{2.2}$$

where σ_c is the conductivity of copper and k_{def} is a defection factor that represents how well the conductive ink behaves compared to the copper. It has been determined through experimental study that k_{def} is approximately 1/200 for the inkjet printed antenna. Based on the above formula, at 2.22 GHz, the skin depth is approximately 1.395 µm for the copper antenna and 19.727 µm for the printed antenna.

To understand the effect of the ink's conductivity and thickness on the radiation efficiency, HFSS and Advanced Design System (ADS) momentum simulations were performed on an S-band patch antenna (Fig. 2.52) using metallic materials with different conductivity values. Table 2.3 lists the HFSS simulation results. Copper/10, Copper/100, and Copper/200 indicate the patch materials with 1/10, 1/100, 1/200 conductivity of the normal copper, respectively. The sixth row of the Table 2.3 models the inkjet printed antenna. Typically, the print is about 500-1000 nm, and if 500 nm is taken as the thickness of one layer of conductive ink on the PET film, printing five times gives a printed pattern with a 2.5 µm of ink thickness. Therefore, a metallic material with a thickness of 2.5 µm and a conductivity of 1/200 of copper can be a good model for the inkjet printed patch antenna.

The antenna dimensions are the same in all the simulations listed in the tables. From the simulation results in Table 2.3 it can be concluded that, when the patch metal thickness is kept the same (rows 1-5), the directivity is almost a constant regardless of patch

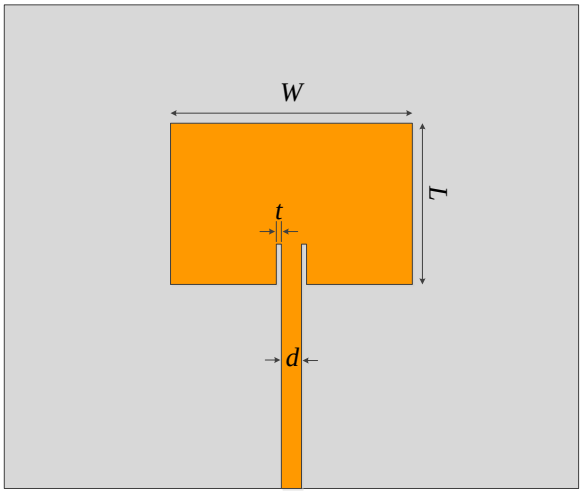

Fig. 2.52: Inset-fed S-band patch antenna geometry.

Table 2.3: HFSS simulation results.

Patch material	Patch thks (µm)	δ (µm)	Freq. (GHz)	S11 (dB)	D_0 (dB)	G_0 (dB)	Eff. (%)
Pec	34=∞ δ	0	2.222	-27.09	7.54	7.43	95.79
Copper	34=24δ	1.395	2.221	-26.14	7.67	7.35	92.75
Copper/10	34=7.7δ	4.411	2.220	-37.34	7.67	7.00	85.88
Copper/100	34=2.4δ	13.949	2.216	-21.16	7.62	6.03	69.49
Copper/200	34=1.7δ	19.727	2.216	-17.32	7.57	5.44	61.23
Copper/200	2.5=0.13δ	19.727	2.216	-15.90	7.52	5.32	60.04
Copper/200	0.5=0.025δ	19.727	2.216	-15.78	7.54	5.32	60.01

material conductivity. However, when the conductivity decreases, the efficiency decreases significantly. As a result, the gain decreases as well. Also, the input impedance decreases as the conductivity decreases, which creates the variation of the S11 values listed in the table. From rows 5-7, a slight decrease in the efficiency can be seen when the antenna's thickness is reduced to below the skin depth.

It is well known that a finite element method based simulator like HFSS is not accurate for thin structures. To better understand the effect of the patch's thickness that is close to or lower than its skin depth, similar simulations were performed in ADS momentum. The results are listed in Table 2.4. The ADS simulation results in rows 1-3 confirm the conclusion drawn from HFSS simulations in Table 2.4 that reduced conductivity decreases the radiation efficiency significantly. The results in rows 3-7, where the thickness of the Copper/10 material is reduced, indicate that the thickness of the patch does have significant effect on antenna performance as well. Therefore, increasing the conductivity and thickness of the ink is the key to improve the inkjet printed antenna performance.

Table 2.4: ADS momentum simulation results.

Patch material	Patch thks (µm)	δ (µm)	Freq. (GHz)	S11 (dB)	D_0 (dB)	G_0 (dB)	Eff. (%)
Pec	$34{=}\infty\ \delta$	0	2.244	-17.73	6.97	6.29	85.98
Copper	$34{=}24\delta$	1.395	2.244	-16.78	6.98	6.14	82.86
Copper/10	$34{=}7.7\delta$	4.411	2.243	-15.27	6.96	5.93	78.84
Copper/10	$22.055{=}5\delta$	4.411	2.243	-15.39	6.98	5.88	78.07
Copper/10	$4.411{=}1\delta$	4.411	2.244	-14.71	6.98	5.73	75.31
Copper/10	$2.205{=}0.5\delta$	4.411	2.244	-13.05	6.99	5.30	68.16
Copper/10	$0.411{=}0.1\delta$	4.411	2.245	-7.74	7.05	2.43	34.57

Chapter 3

Wraparound S-Band and GPS Antenna Arrays for Sounding Rocket Sub-Payload

This chapter presents the detailed antenna design for a sub-payload. The inkjet printing method introduced in Chapter 2 was conveniently applied in validating some of the antenna design.

3.1 Project Overview

The Utah State University Space Dynamics Lab has been undertaking a mission – the NASA Auroral Spatial Structures Probe (ASSP) – to measure both the spatial and temporal variation of the energy flow into the upper atmosphere in and around the aurora. ASSP is the first NASA sounding rocket mission to make use of a constellation of mini-payloads to observe both the spatial pattern and temporal variations associated with this energy. The energy flow, computed from both of these measurements, will allow scientists at Utah State University to understand when and where the Earth's thermosphere will heat and expand due to the Joule heating process. The end result will be an increased understanding of Joule heating and ultimately the processes that lead to global temperature changes in the thermosphere.

ASSP will be launched from Poker Flat Alaska into active aurora during geomagnetically active conditions and just before the onset of an auroral sub-storm. To capture the data, ASSP will use a constellation of six small identical sub-payloads that separate relative to each other throughout a sounding rocket flight. Each sub-payload (Fig. 3.1) is a cylindrical structure with a diameter of six inches and a height of four inches. The cylindrical sub-payload has four booms coming out from the surface as shown in Fig. 3.2. They are metal wires covered by dielectric materials, each of which is two meters long when fully

deployed and one meter long when half deployed. The booms are packaged inside the sub-payload before it is launched and will be deployed after the sub-payloads are detached from the rocket.

The project objective is to design antennas for such a cylindrical sub-payload. It is required to have two types of antennas: one is an S-band antenna and the other is an L-band antenna. The S-band antenna is used for communication between the payloads and the ground stations, and the L-band antenna is used to locate the sub-payload position because it is important to know the exact location where the measurement data is obtained. Each sub-payload will have a slightly different S-band frequency: there are six evenly spaced bands between 2210 - 2230 MHz with the voltage standing wave ratio (VSWR) <2:1, each for one sub-payload. The L band antenna is a GPS antenna. It needs to be RHCPd with a bandwidth of 10 MHz and VSWR <1.5:1 at the center frequency of 1575.42 MHz. The radiation patterns of both types of antennas have to be omni-directional with at least -8 dB gain over the boresight direction (nulls no worse than -8 dB). Besides, the number of ports used to feed the antennas should be minimized to two: one for S-band antenna and the other for GPS antenna. Also, -40 dB of isolation is required between the S-band and L-band antennas.

3.2 S-Band Patch Antenna Array Design

Due to the relatively short traveling distance, the sub-payload system does not need solar cells for energy supply. Instead, a battery is installed inside the cylindrical structure. Therefore, the sub-payload surface is available for the antennas to be mounted on. The geometry of the sub-payload surface determines that the antenna has to be made conformal to the cylindrical surface. Also, the cost and the ease of fabrication and installation require that the antenna has to be low-cost and low-profile.

A microstrip antenna, also called patch antenna, is a thin metallic strip placed above the ground plane, with a substrate in between [12]. It is widely used in aircraft, spacecraft, satellite, and missile applications where a low-profile, low-cost, easy-to-fabricate, conformal to non-planar surfaces, robust antenna is needed [12]. A patch antenna can be made in

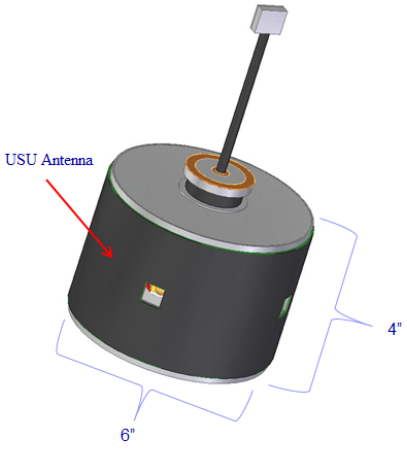

Fig. 3.1: Sub-payload without booms.

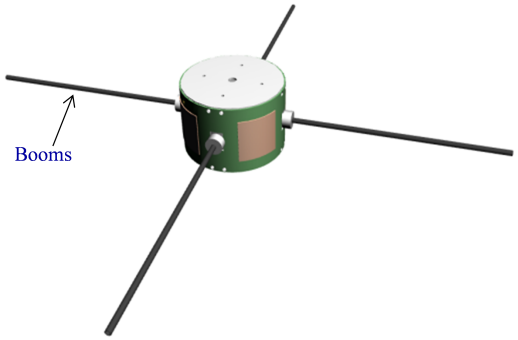

Fig. 3.2: Sub-payload with booms.

various shapes such as rectangular, circular, triangular, etc. However, the rectangular patch is the most widely used configuration and gives LPd radiation if no geometrical modification is applied [12]. Considering the above mentioned advantages, a rectangular patch was chosen as the sub-payload LPd S-band antenna.

3.2.1 Initial Study of S-Band Antenna Design

Figure 3.3 shows the geometry of the S-band rectangular patch antenna. Its design center frequency was chosen as 2.225 GHz, which is the average of the S-band antenna bandwidth (2210 - 2230 MHz). Initial dimensions of the patch antenna were calculated using the Transmission-Line Model and then tuned to the right center frequency using HFSS. To make it conformal to the sub-payload surface, the length (L) of the patch was adjusted to compensate the bending effect as there will be a frequency shift when the planar patch is wrapped around a cylindrical surface [10].

A single patch antenna has directional radiation pattern with a 3 dB beamwidth of around 60°. In order to design an omnidirectional S-band antenna, more patches should be placed on the cylinder's surface with a certain distance among them. The dimension of the sub-payload (six inches in diameter and four inches in height) determines that, at most, four S-band and four GPS patches can be mounted on the cylinder's surface. A two-

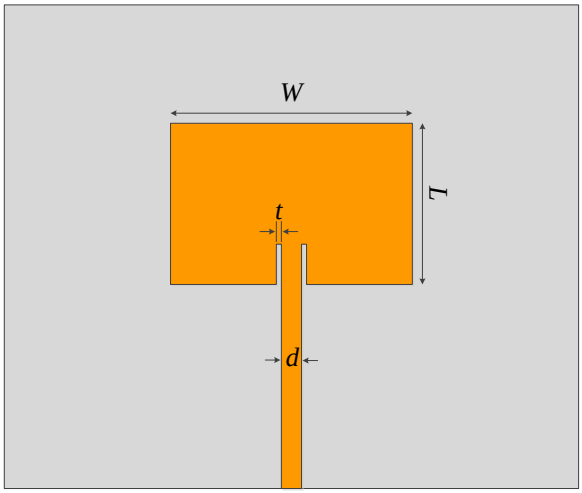

Fig. 3.3: Inset-fed S-band patch antenna geometry.

element S-band antenna array cannot provide an onmidirectional radiation pattern as each one of the patches is not able to cover 180° of space with -8 dB gain over the the boresight. A three-element S-band antenna array (Figs. 3.4-3.5) was also designed in HFSS, and its radiation pattern on the boresight was omnidirectional as shown in Fig. 3.6. However, it was found difficult to assure that the three feed lines, which go from the port to the patches, have the same length. Although this could be done in simulation, it was expected that it would be hard to do so in fabrication. In addition, the actual positions of the four booms would make it difficult to place the patches symmetrically around the cylinder surface. Unequally spaced patches, on the other hand, would distort the onmidirectional property of the three-element array and would also introduce more meander lines on the surface to keep the same current phase for each patch element.

3.2.2 Finalized S-Band Antenna Design

As it can be seen from Fig. 3.2, the four booms are symmetrically positioned on the cylinder's surface: they divide the cylinder surface into four identical sectors. Therefore, a four-element antenna array can be placed symmetrically around the surface, which makes the feed line design relatively simple. At first, a four-element S-band antenna array with separate feed lines (Fig. 3.7) was designed in HFSS without considering the complex feed

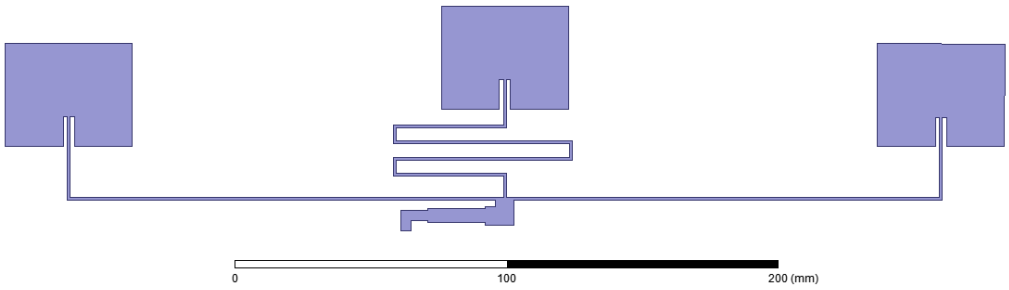

Fig. 3.4: Three-element planar antenna array.

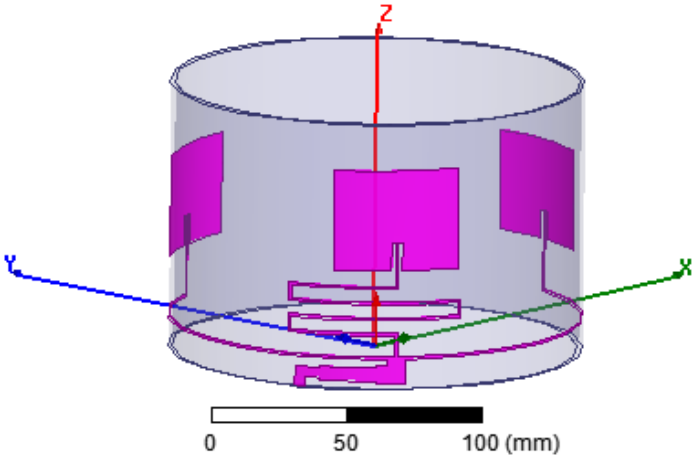

Fig. 3.5: Three-element conformal antenna array.

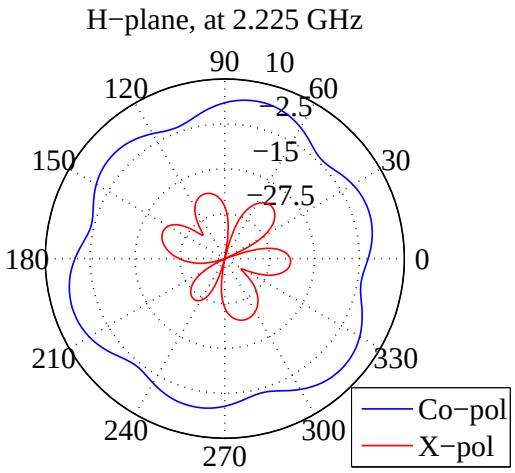

Fig. 3.6: Simulated H-plane radiation pattern of the three-element array.

line. Figure 3.8 shows its radiation pattern on the boresight. It can be seen that the radiation pattern of the four-element array is omnidirectional, with minimum -2.5 dB of gain on the boresight, which satisfies the project requirement of minimum -8 dB of gain.

3.3 Feed Line Interference

In order to have only one port for the S-band antennas, it is necessary to design a feed line connecting the four patches together to a single input port. This involves impedance transformation between transmission lines that have different characteristic impedances. The planar antenna structure with the complex feed line is shown in Fig. 3.9. Looking from the port, the transmission line starts with the characteristic impedance of 50 Ω, which is the most commonly used standard value. It is then divided into two 100 Ω transmission lines. They should be divided further into four branches, but the width of the 100 Ω transmission line is 1.045mm, which is already quite thin. Since the width of a microstrip line decreases as its characteristic impedance increases, it is necessary to use an impedance transformer to transform the 100 Ω transmission line into 50 Ω transmission line. A quarter-wave impedance transformer has been chosen for that as it has the simplest configuration and shortest length. Through the transformer, the two 100 Ω transmission lines are transformed into two 50 Ω transmission lines, and they are then divided into four 100 Ω transmission lines, each for one patch. Figure 3.10 shows the conformal antenna structure, which is made by wrapping the planar antenna structure on the cylinder surface.

It is seen from Fig. 3.8 that the four-element S-band array produced a nice onmidirectional radiation pattern when the patches were fed separately. However, when the complex feed line was placed on the cylinder surface together with the patches, unexpected S11 (Fig. 3.11) and radiation pattern (Fig. 3.12) were observed in the simulation. In order to verify the simulation results in a fast manner, the inkjet printing method was used for antenna prototyping. Figure 3.13 shows the inkjet printed four-element S-band antenna array wrapped on the cylindrical surface. The measured radiation pattern is shown in Fig. 3.14, which agrees well with the simulated radiation pattern in Fig. 3.12. This proves that the feed line is interfering with the antenna's radiation.

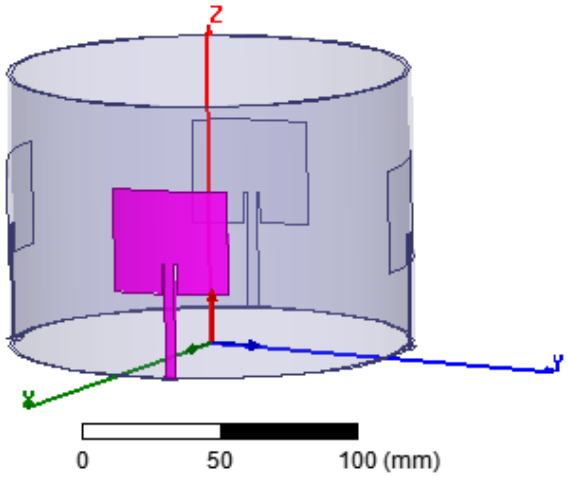

Fig. 3.7: Four-element conformal antenna array.

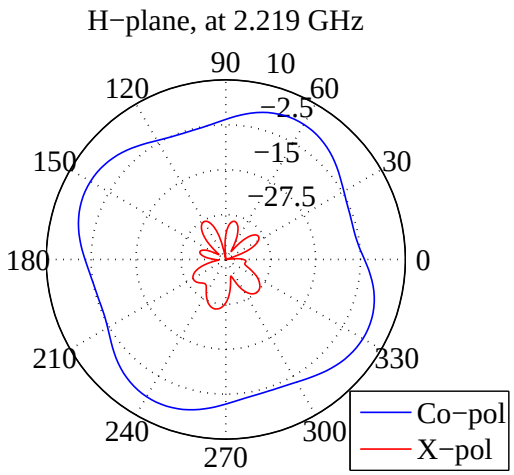

Fig. 3.8: Simulated H-plane radiation pattern of the four-element array.

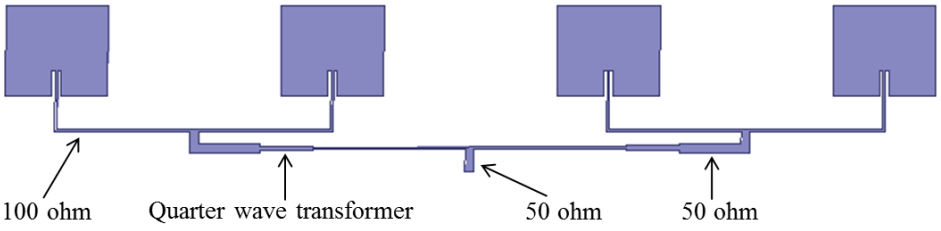

Fig. 3.9: Four-element planar antenna array.

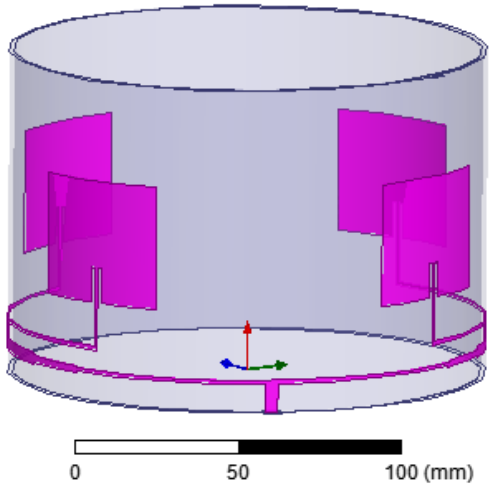

Fig. 3.10: Four-element conformal antenna array.

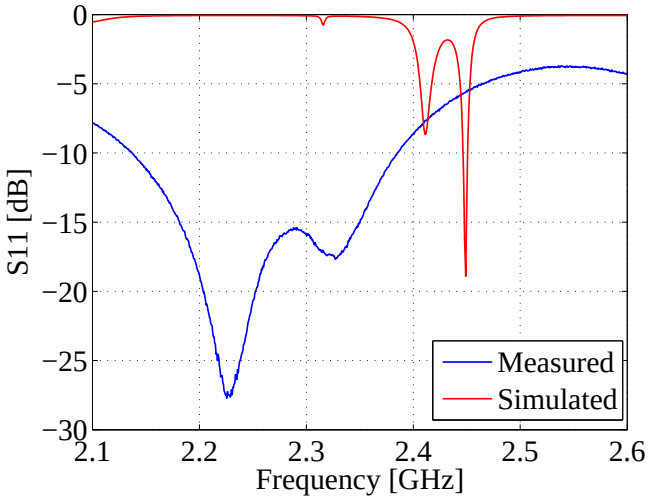

Fig. 3.11: S11 of the printed antenna.

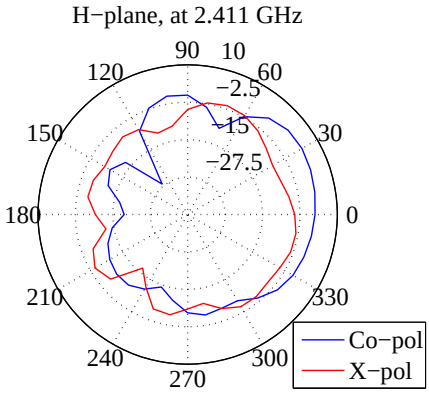

Fig. 3.12: Simulated H-plane radiation pattern of the printed antenna.

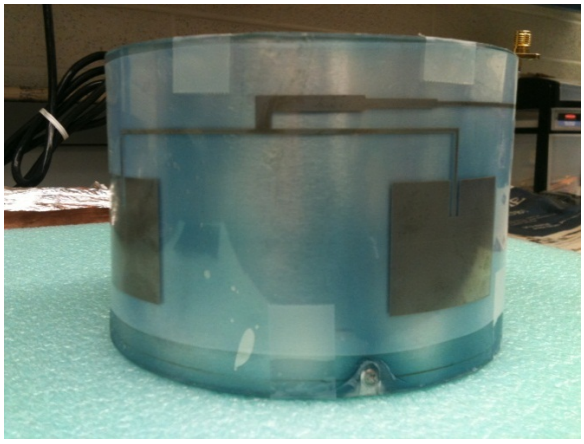

Fig. 3.13: Printed four-element conformal antenna array.

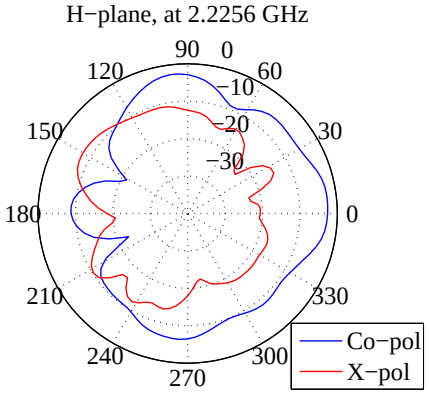

Fig. 3.14: Measured H-plane radiation pattern of the printed antenna.

To further comprehend the problem of feed line interference, two two-element S-band arrays were inkjet printed. They were then assembled on the surface and connected using a two-way power divider as shown in Figs. 3.15-3.16. The S11 and radiation patterns are given in Figs. 3.17-3.19. As can be seen, the measured results agree well with the simulation. The frequency shift is due to the PET film, scotch tape, and the power divider, which were not included in the HFSS simulation. Also, there could have some air between the patch and the substrate when the antenna was taped on the substrate. This testing result shows that the radiation interference is mainly caused by the microstrip line connecting the two two-element antenna arrays.

3.4 Multilayer Antenna Structure

Since the radiation interference is happening between the feed line and the patches, it is necessary to hide the feed line and shield it from the patches. As one way of realizing that, the multilayer antenna structure shown in Fig. 3.20 is proposed, where the feed line is placed in a different layer from the patches with metal shielding between them. The components from the bottom to the top are, respectively, first layer of ground plane, first layer of G10, feed line, second layer of G10, second layer of ground plane, RT6002 antenna substrate, and the patch. The feed line is connected to the patch through a via. The two ground planes will be connected through many vias in the real fabrication. Since the feed line is placed between the two ground planes, it becomes a strip line instead of a microstrip line. Therefore, the feed line should be designed using strip line designing principle.

Based on the above mentioned multilayer concept, the cylindrical multilayer antenna structure was designed in HFSS as shown in Fig. 3.21. To make the design more rigorous, the four-element GPS antenna array and the complex feed lines of the S-band and GPS antenna arrays were also included. A cylindrical antenna structure with the two types of antennas fed by separate probe feeds was also designed as a reference (Fig. 3.22). Since the feed lines were separated from the patches by a metal ground plane and connected to the patches through vias, the feed line layers (two G10 layers and the striplines) of the reference antenna structure were simplified as separate probe feeds. It is seen from Fig. 3.23 that the

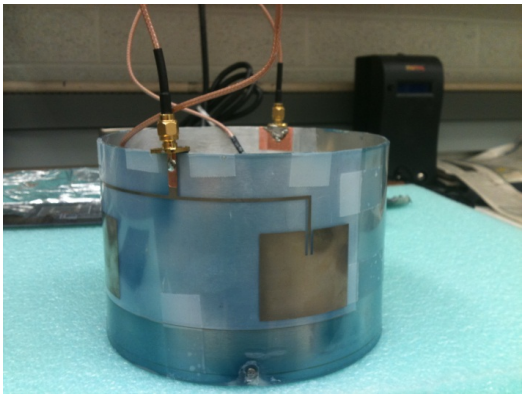

Fig. 3.15: Printed antenna arrays (front view).

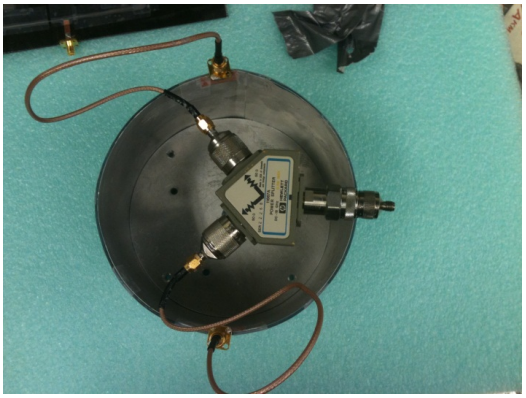

Fig. 3.16: Printed antenna arrays (top view).

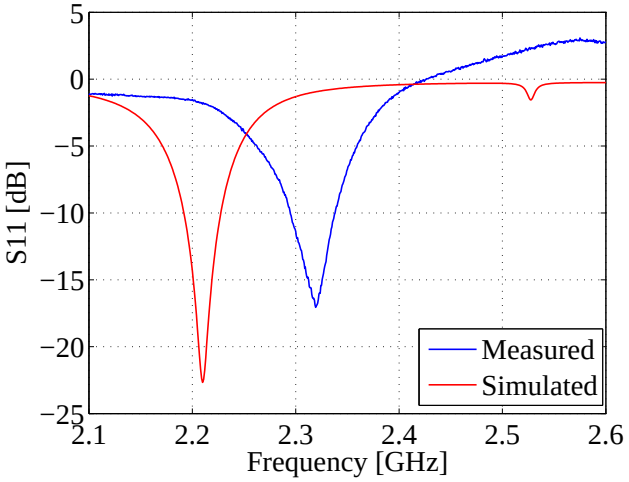

Fig. 3.17: S11 of the two two-element printed antenna arrays.

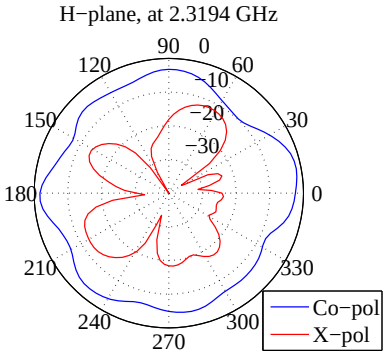

Fig. 3.18: Measured H-plane radiation pattern of the printed antenna.

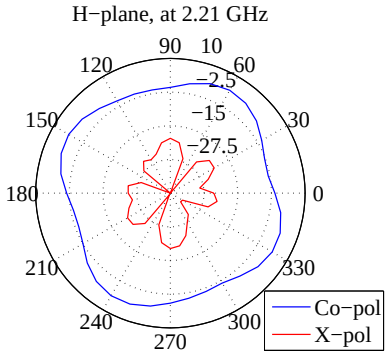

Fig. 3.19: Simulated H-plane radiation pattern of the printed antenna.

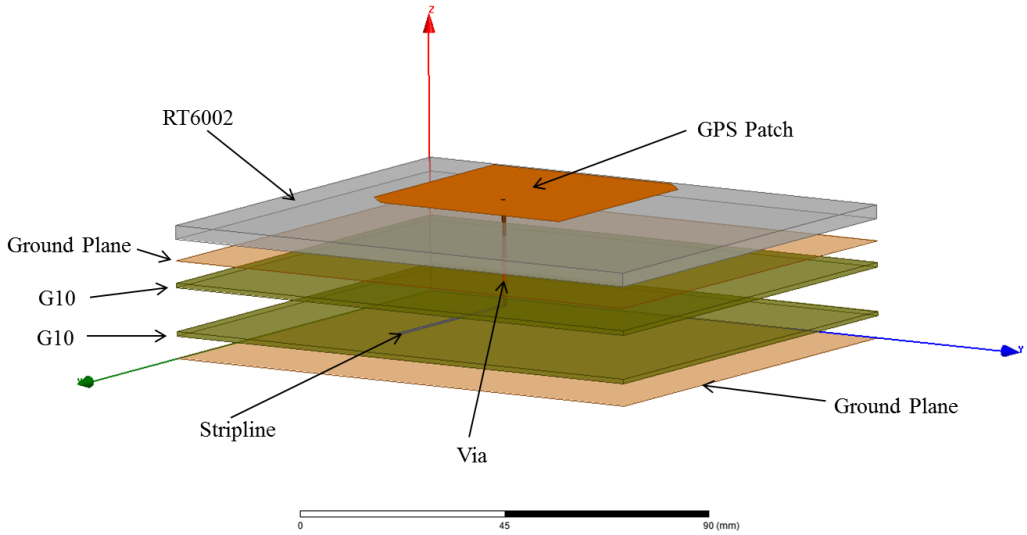

Fig. 3.20: Multilayer antenna structure.

simulated S-band radiation pattern of the actual multilayer structure is omni-directional, which is almost the same as, or even better than that of the reference antenna (Fig. 3.24). This clearly shows that the proposed multilayer structure solves the feed line interference problem.

3.5 Boom Effect

The cylindrical sub-payload has four booms coming out from the surface as shown in Fig. 3.25. They are metal wires covered by dielectric materials. Each boom is two meters long when fully deployed and one meter when half deployed. It is obvious to expect that such a metal boom structure will affect the antenna performance. In order to understand the boom effect, a simple study was carried on a single LPd planar GPS antenna with the boom placed in different positions as shown in Figs. 3.26-3.27. From Fig. 3.26, in which the boom is placed in its actual position, it is obvious that the principal E-plane is parallel to the boom. In this case, it is expected that the effect of boom on the radiation pattern of antenna will be negligible. On the other hand, if the boom is on the same plane with the principal E-plane as shown in Fig. 3.27, it will disturb the E-filed by canceling out its vertical portion and will cause some perturbation in the radiation pattern. From this

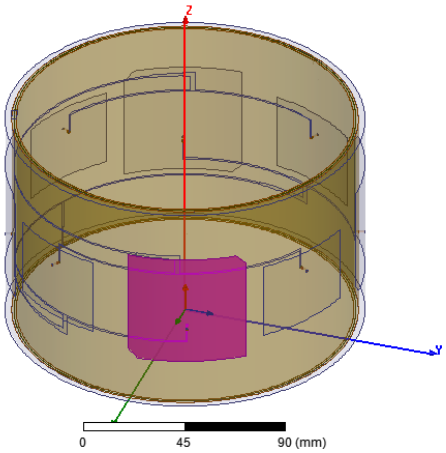

Fig. 3.21: Actual multilayer antenna structure.

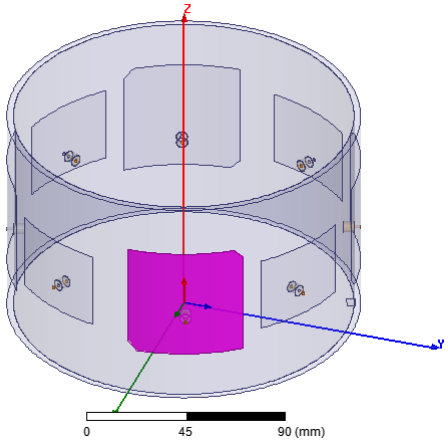

Fig. 3.22: Simplified multilayer antenna structure.

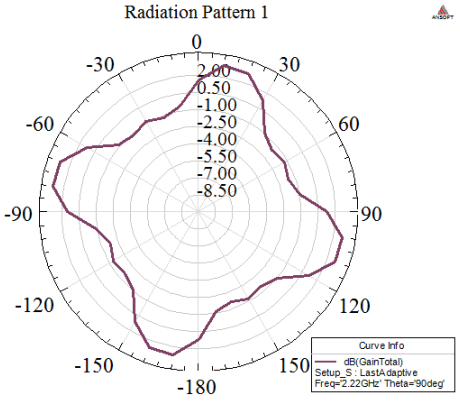

Fig. 3.23: H-plane radiation pattern of the actual multilayer structure.

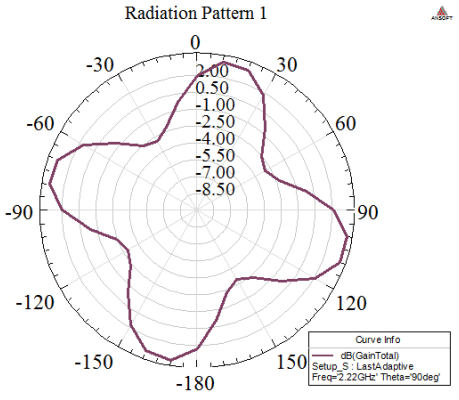

Fig. 3.24: H-plane radiation pattern of the simplified multilayer structure.

analysis it can be concluded that the boom has negligible effect on the S-band antenna as it is LPd. However, since the CPd GPS antenna utilizes all of its edges, the boom will introduce some distortion to the radiation pattern of the GPS antenna.

In order to verify the conclusions drawn from the above boom effect analysis, HFSS simulations for three different cases were performed as shown in Fig. 3.28. Their corresponding E-plane and H-plane radiation patterns are shown in Fig. 3.29, where it can be seen that the boom has little effect on the LPd S-band radiation pattern because of its practical position; however, it tilts the radiation pattern when placed near the adjacent patch edge. Also, it can be concluded from the S11 plots in Fig. 3.30 that boom position has no effect on the resonant frequency of the LPd S-band antenna.

In the same manner, similar HFSS simulations were also performed for the CPd GPS antenna, as shown in Fig. 3.31, to see the boom effect on its performance. The corresponding radiaion patterns, S11, AR in frequency domain, and AR on the E-plane are shown in Figs. 3.32-3.35, respectively. It can be observed that the boom has little effect on the resonant frequency and AR frequency; however, it tilts the radiation pattern and changes the AR value at a certain angle position for a given frequency.

From the theoretical analysis and simulation results it can be concluded that the boom has little effect on the radiation pattern of the LPd S-band antenna but has clear effect on that of the CPd GPS antenna. Also, it has negligible effect on the resonant frequency of both S-band and GPS antennas. Although the boom has little effect on AR frequency, it changes the AR value at a certain angle position for a given frequency. It should be noted that the above conclusions were made while the boom length was taken as 85 mm in order to reduce the HFSS simulation time.

3.6 Circularly Polarized GPS Patch Antenna Design

This particular sub-payload has to receive GPS signal to locate its position. To better discriminate between the direct and reflected signals, the GPS satellites transmit RHCPd signals, which has the property of becoming left-handed circularly polarized after the reflection on the ground [15]. For that reason, the GPS antenna of this sub-payload is preferred

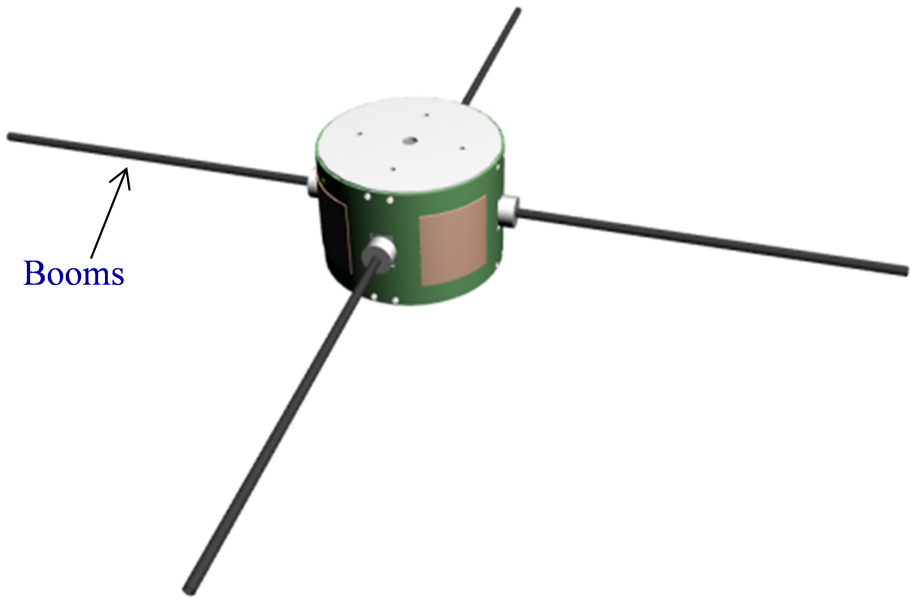

Fig. 3.25: Sub-payload with wire booms.

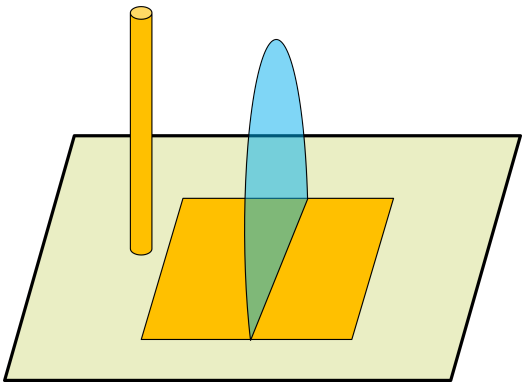

Fig. 3.26: Boom near the patch length.

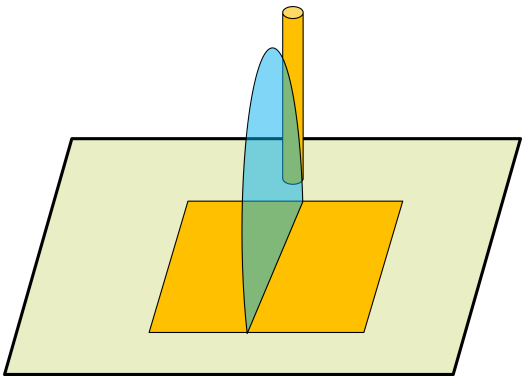

Fig. 3.27: Boom near the patch width.

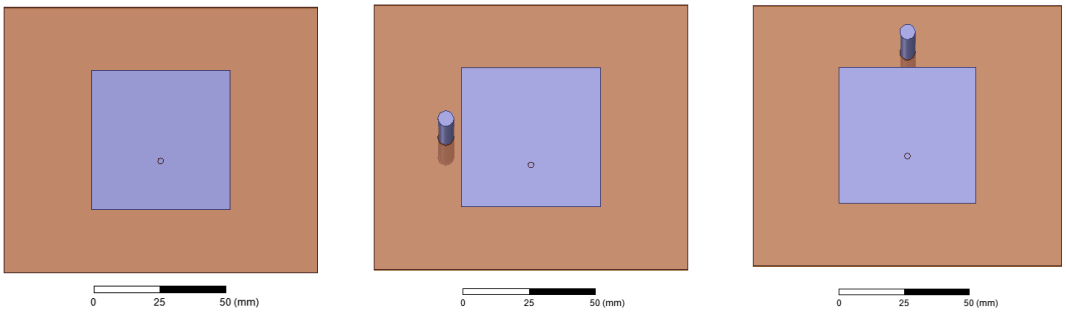

(a) (b) (c)

Fig. 3.28: Patch antennas with or without booms.

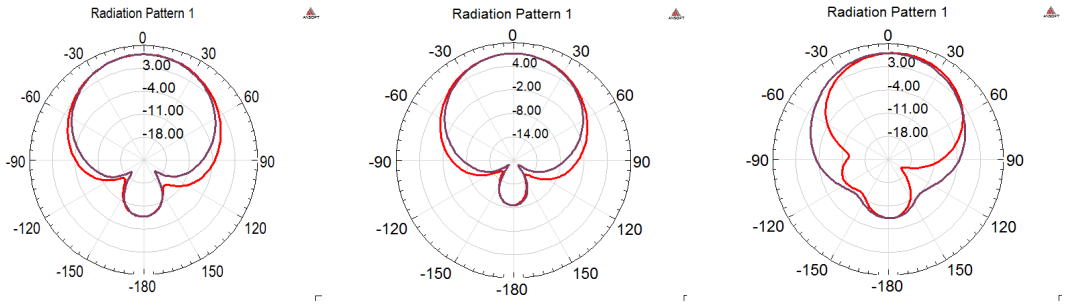

(a) (b) (c)

Fig. 3.29: E-plane and H-plane radiation patterns of the above three antennas.

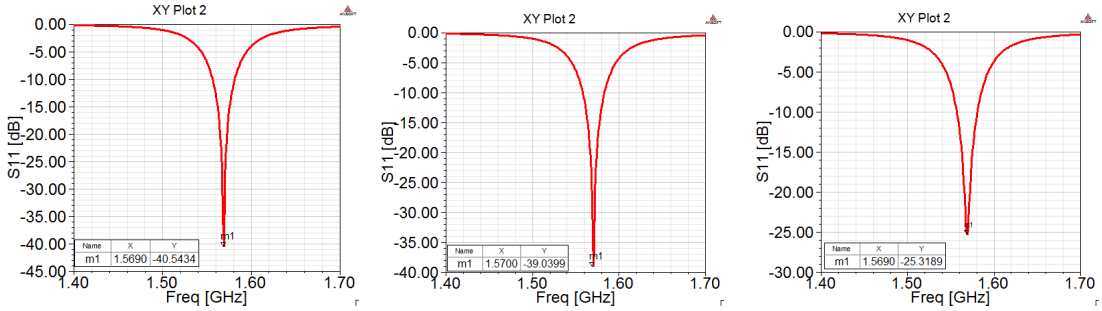

(a) (b) (c)

Fig. 3.30: S11 of the above three antennas.

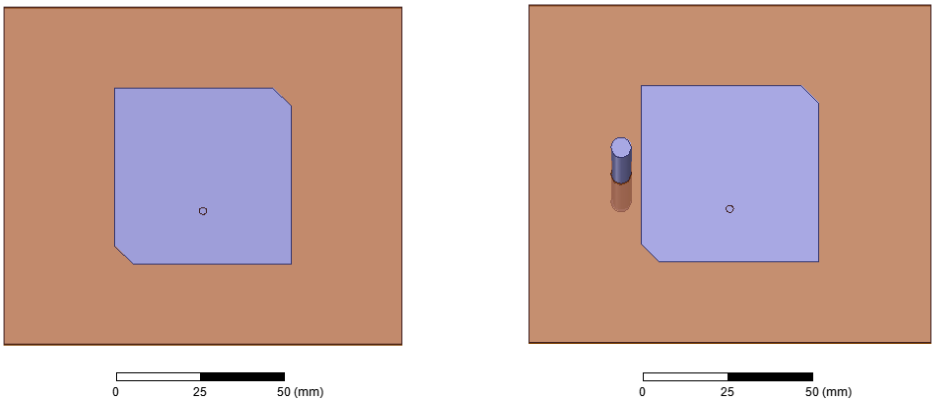

(a) (b)

Fig. 3.31: CPd GPS patch antenna with and without the boom.

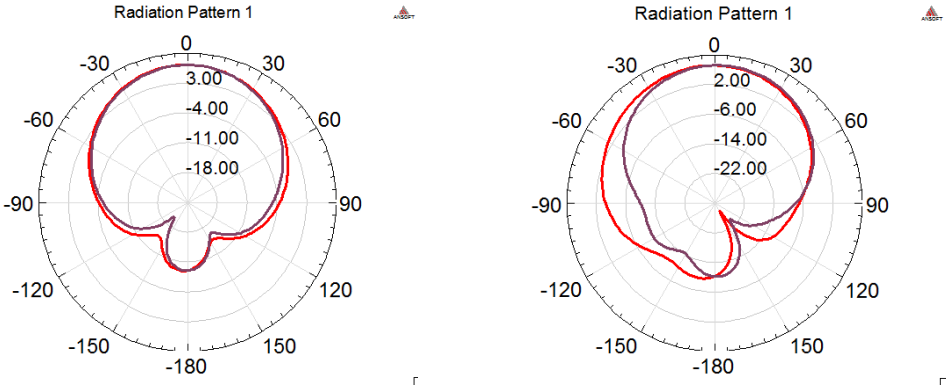

(a) (b)

Fig. 3.32: E-plane and H-plane radiation patterns of the above two CPd GPS antennas.

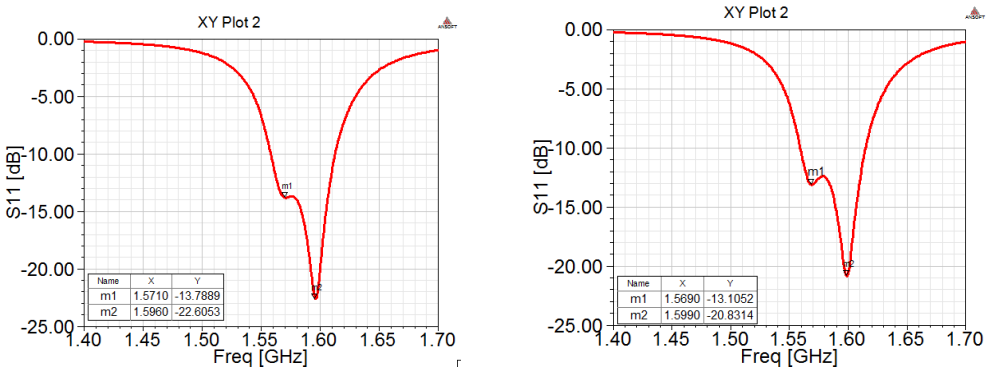

(a) (b)

Fig. 3.33: S11 of the above two CPd GPS antennas.

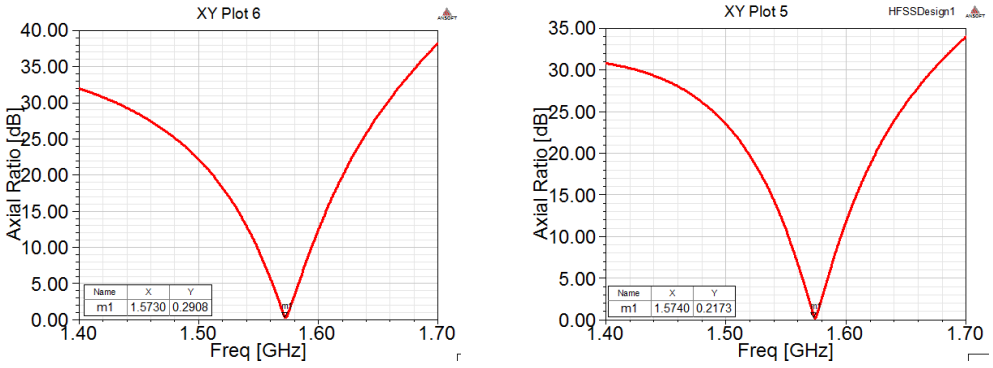

(a) (b)

Fig. 3.34: Axial ratio of the above two CPd GPS antennas.

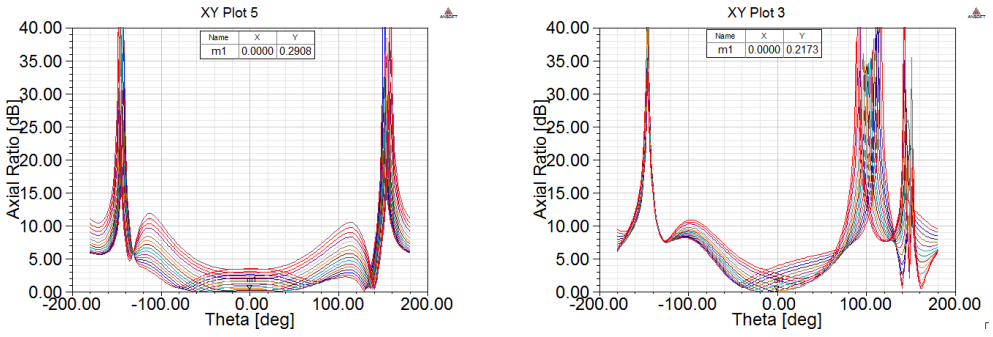

(a) (b)

Fig. 3.35: Axial ratio of the above two GPS antennas on E-plane, from 1.565 - 1.580 GHz.

to be RHCPd. Since the antenna is mounted on the sub-payload outer layer, the GPS antenna has to be conformal to the cylindrical surface. It is known that when bending a planar CP antenna onto a cylindrical surface, the CP property is easily lost [16]. Therefore, it is important to study a reliable CPd conformal antenna. Most reported cylindrical CPd antennas have relatively complex antenna geometries [17–19] and are not suitable for the sub-payload. On the other hand, a microstrip patch antenna with a simple feed is a better solution, as the bandwidth requirement of the sub-payload antenna is low and the main objective is the ease of fabrication.

3.6.1 Single GPS Patch Antenna Design

The basis of the antenna design is the planar probe-fed CPd design as shown in Fig. 3.36. The two truncated corners result in two orthogonal modes with 90° of phase shift [13]. The angle of the corner truncation is 45°, which is the same for both planar and cylindrical cases. Also, the truncation on the two corners are identical. As a starting point, a single CPd GPS patch antenna was design at the center frequency of 1.575 GHz, whose length, width, and the amount of truncation are 53.15 mm, 53.15 mm, and 5.5 mm, respectively; and the distance between the pin center and the lower edge of the patch is 16 mm. The S11 and AR plots are shown in Figs. 3.37-3.38. It should be noted that the polycarbonate was used as the antenna substrate since the cost is low, and it is easy to be wrapped around a cylindrical structure. The thickness of the substrate is 1.524 mm and the permittivity is 2.9.

When the planar structure is transformed to a cylindrical surface, the antenna geometry must be adjusted in order to maintain a good CP. The bending has two effects on the CPd antenna: (1) it shifts the center frequency, (2) CP gets deteriorated [14, 16, 20, 21]. For the frequency shifting, the antenna dimensions have to be adjusted to offset the shift in resonance frequency. As for the damaged CP, the amount of corner truncation has to be tuned. It is also helpful to make the patch nearly square while trimming the corners. Based on the above tuning method, a conformal CPd GPS antenna (Fig. 3.39) was designed at the center frequency of 1.575 GHz. The antenna's width and length are the same, 53.65

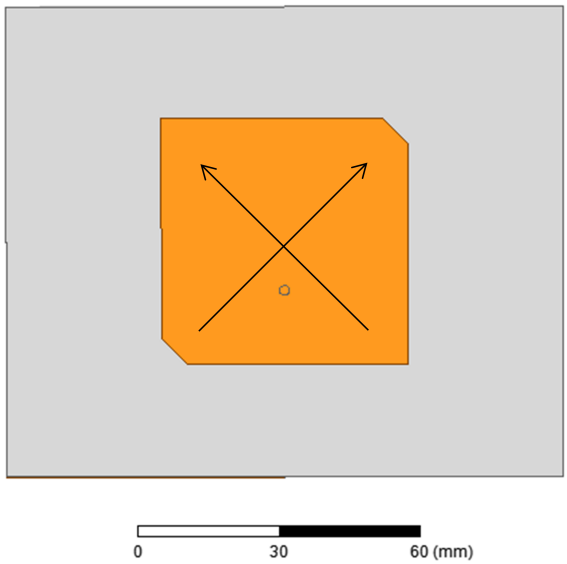

Fig. 3.36: CPd GPS patch antenna.

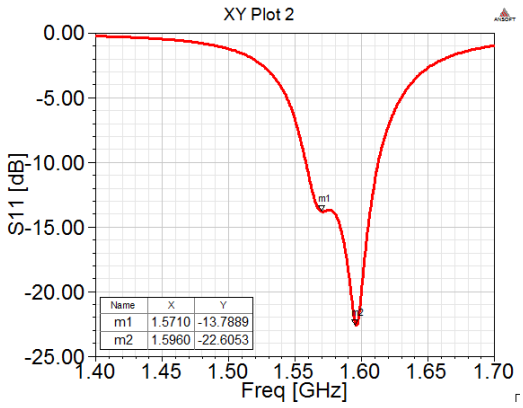

Fig. 3.37: S11 of the CPd GPS antenna.

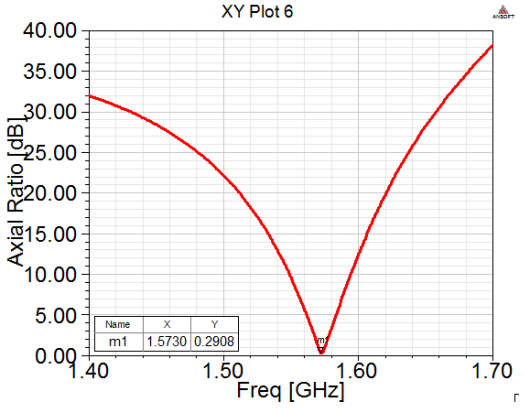

Fig. 3.38: AR of the CPd GPS antenna.

mm, the amount of truncation is 5.75 mm, and the distance between the pin center and the lower edge of the patch is 16 mm. The simulated S11, AR and radiation pattern are shown in Figs. 3.40-3.43. The best CP is at 1.582 GHz with the AR of 1.11.

The same structure as shown in Fig. 3.39 was simulated with the booms placed in their actual positions. It should be noted that short booms with 85 mm of length were used in the simulation since such a cylindrical structure with the actual boom length (two meters) made the HFSS simulation extremely time consuming. Figure 3.44 shows the geometry of the structure. The antenna's width and length are the same, 53.65 mm, the amount of truncation is 5.75 mm, the distance between the pin center and the lower edge of the patch is 16 mm. The simulated S11, AR plots and radiation pattern are shown in Figs. 3.45-3.48. It can be observed that the radiation pattern gets distorted because of the booms. Also, the AR value increases without any further tuning, and the best AR frequency is decreased to 1.578 GHz with the AR of 0.71.

3.6.2 Four-Element GPS Patch Antenna Array Design

The single CPd conformal GPS patch antenna was extended to a four-element CPd GPS antenna array. They were placed symmetrically on the cylinder surface without the booms as shown in Fig. 3.49. From the simulation it was observed that the center frequency increases compared to the single CPd conformal GPS antenna with the same antenna dimensions. The frequency shift was tuned by adjusting the length of the antennas, but the

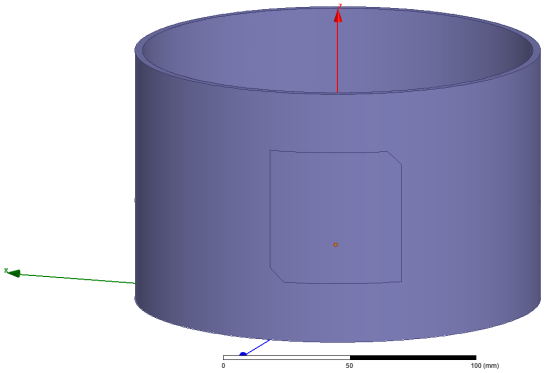

Fig. 3.39: CPd GPS patch antenna.

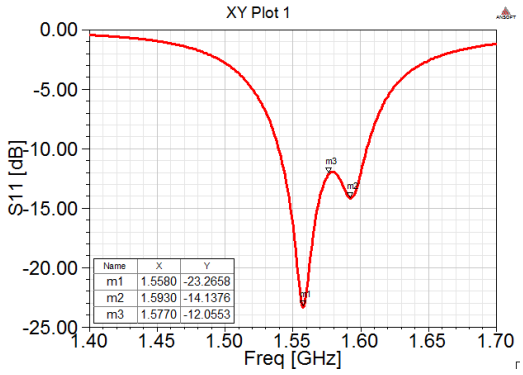

Fig. 3.40: S11 of the CPd GPS antenna.

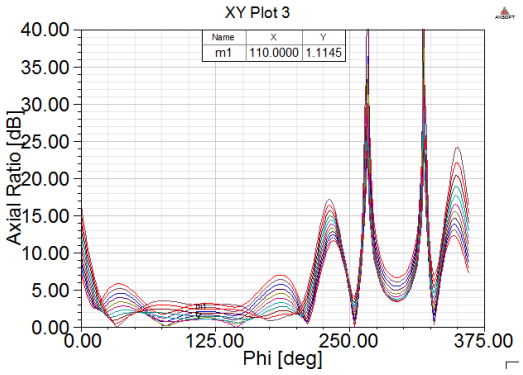

Fig. 3.41: AR, from 1.578 - 1.588 GHz.

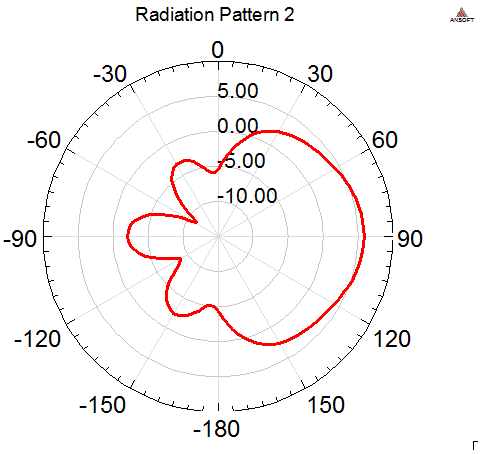

Fig. 3.42: E-plane.

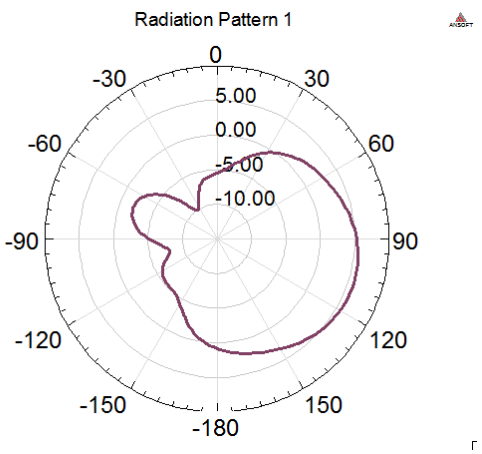

Fig. 3.43: H-plane.

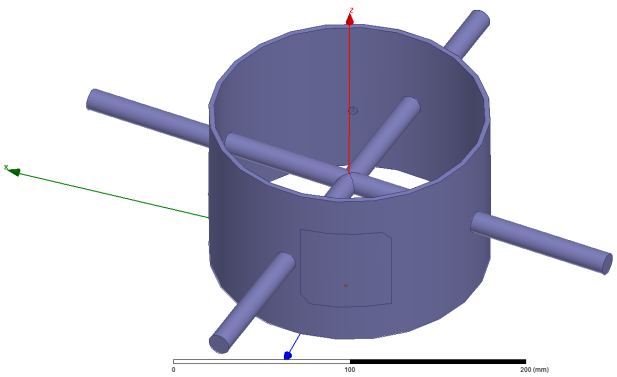

Fig. 3.44: CPd GPS patch antenna with boom.

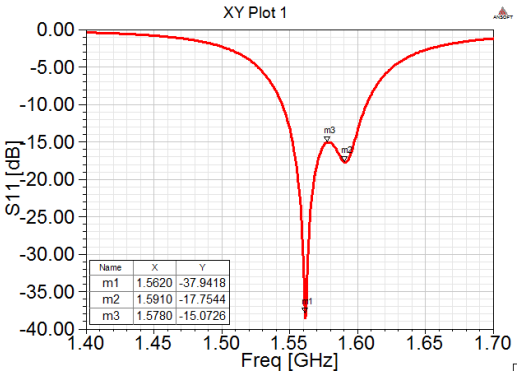

Fig. 3.45: S11 of the CPd GPS antenna.

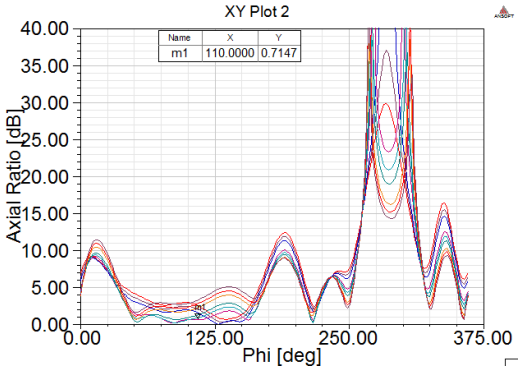

Fig. 3.46: AR, from 1.573 - 1.584 GHz.

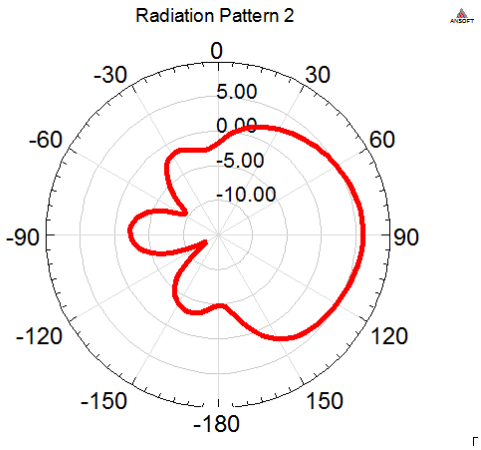

Fig. 3.47: E-plane.

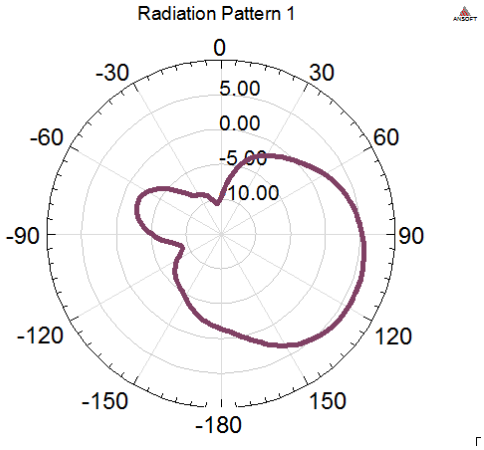

Fig. 3.48: H-plane.

amount of corner truncation was kept the same. The tuned antenna's width, length, and truncated length are 54.25 mm, 54.25 mm, and 5.75 mm, respectively, and the distance between the pin center and the lower edge of the patch is 16 mm. The simulated S11, AR plots and radiation patterns are shown in Figs. 3.50-3.53. It is seen that the radiaton pattern is omni-directional, and the best CP is at 1.585 GHz with the AR of 0.84.

While keeping the antenna dimensions the same, the short booms were then added into the simulation as shown in Fig. 3.54. The simulated S11, AR plots and radiation patterns are shown in Figs. 3.55-3.58. It can be seen that the radiation pattern is still omni-directional, but it has some roughness in it, which can be observed more clearly on the 3-D radiation pattern. This is mainly due to the boom effect as it tilts the radiation pattern. The first resonant frequency increases compared to that in Fig. 3.50, however, the best CP frequency decreases, and the AR value of each angle position changes compared to the case without the booms (Fig. 3.51). The best CP is at 1.57 GHz with the AR of 0.23.

3.6.3 Four-Element GPS Patch Antenna Array Design When Placed with Four-Element S-Band Patch Antenna Array

The four GPS antnenas with their dimensions unchanged were simulated together with the four S-band antennas without including the booms as shown in Fig. 3.59. The simulated S11, AR plots and radiation patterns are shown in Figs. 3.60-3.63. It is seen that the radiation pattern still keeps its omni-directionality. The best CP is at 1.584 GHz with AR

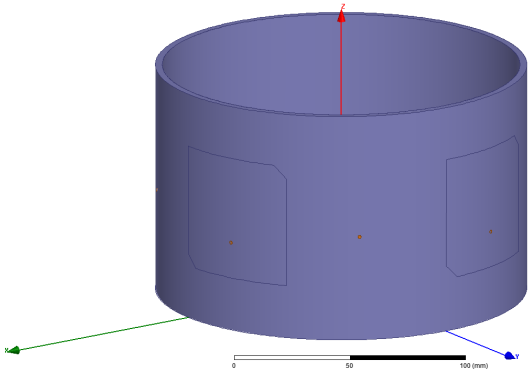

Fig. 3.49: Four-element GPS patch antenna array.

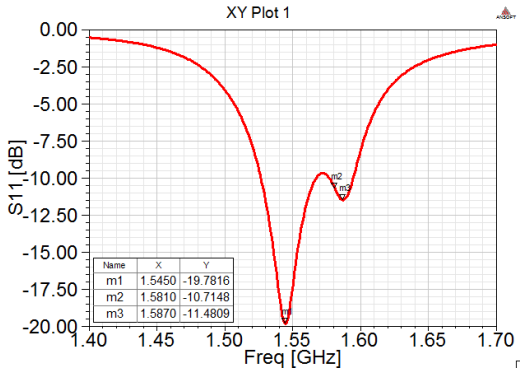

Fig. 3.50: S11 of the CPd GPS antenna.

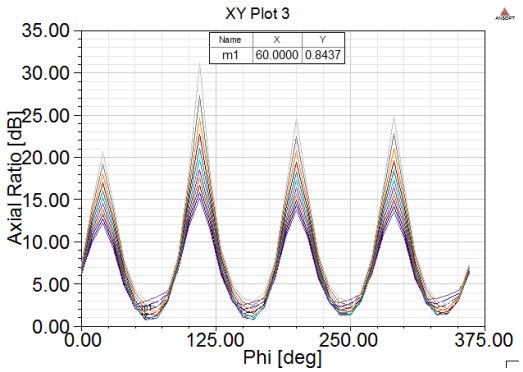

Fig. 3.51: AR, from 1.579 - 1.590 GHz.

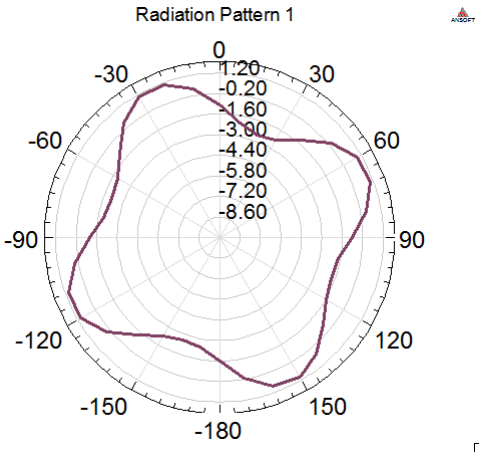

Fig. 3.52: H-plane, boresight.

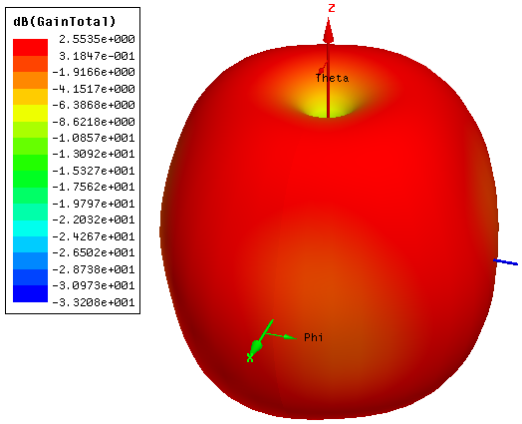

Fig. 3.53: 3-D radiation pattern.

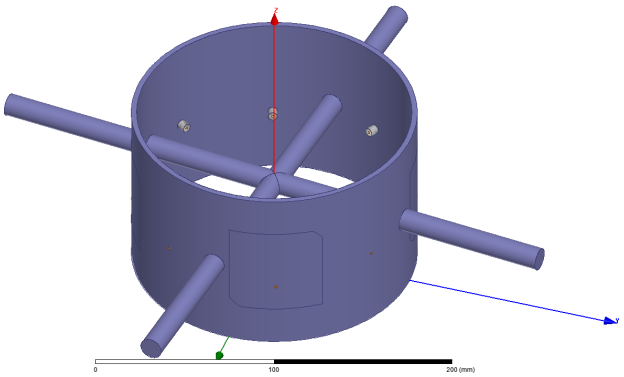

Fig. 3.54: Four-element GPS patch antenna array.

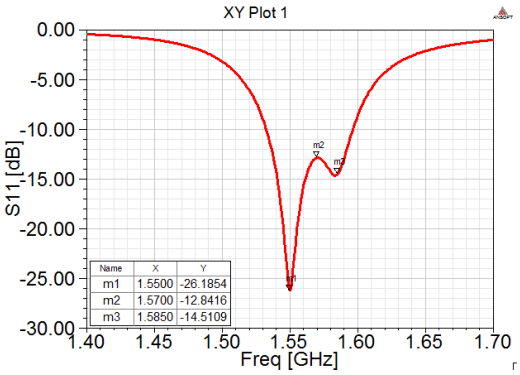

Fig. 3.55: S11 of the CPd GPS antenna.

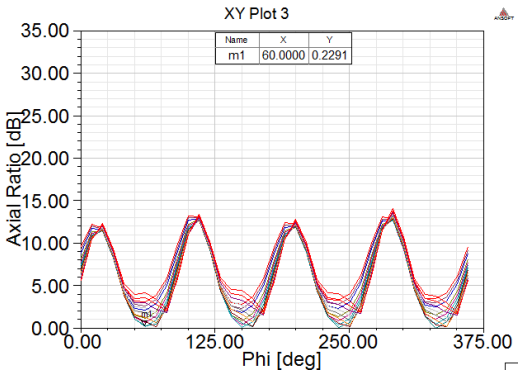

Fig. 3.56: AR, from 1.564 - 1.578 GHz.

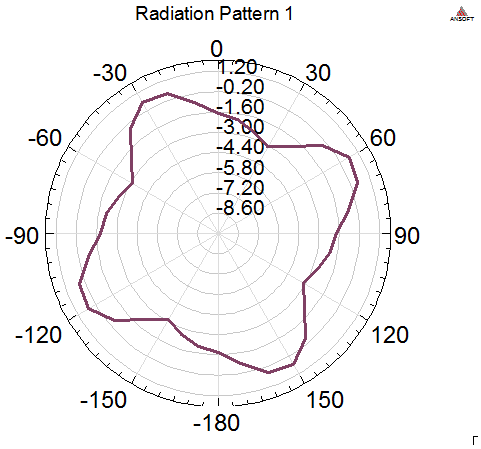

Fig. 3.57: H-plane, boresight.

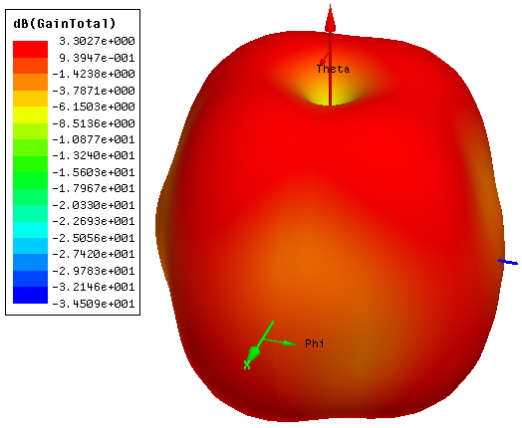

Fig. 3.58: 3-D radiation pattern.

of 1.08. From this it can be concluded that the S-band antenna array has negligible effect on the GPS CP performance.

While maintaining the above antenna dimensions the same, the short booms were added into the simulation as shown in Fig. 3.64. The simulated S11, AR plots, and radiation patterns are shown in Figs. 3.65-3.68. It is seen that the radiation pattern, although distorted a bit, is still omni-directional. The S11 does not change much, however, the best CP frequecy decreases. The best CP is at 1.570 GHz with the AR of 0.35.

Until now the boom length was kept as 85 mm, and the longer booms may have some different effect on the CP performance of the GPS antenna. Therefore, while keeping the dimensions unchanged, the same antenna structure was then simulated with longer booms of length 150 mm (Fig. 3.69), replacing the shorter booms. The simulated S11, AR plots, and radiation patterns are shown in Figs. 3.70-3.73. It is seen that the radiation pattern gets more rougher but is still omni-direstional. The S11 and the best CP frequency were not affected much. The best CP is at 1.573 GHz with the AR of 0.33. However, the longer booms cause the AR value of each angle position to vary from the same simulation with shorter booms.

3.7 Study on Isolation

After the feed line interference problem has been solved, the next challenge is to reduce isolation (S12) level. Since the patches are placed very close to each other, it is quite obvious

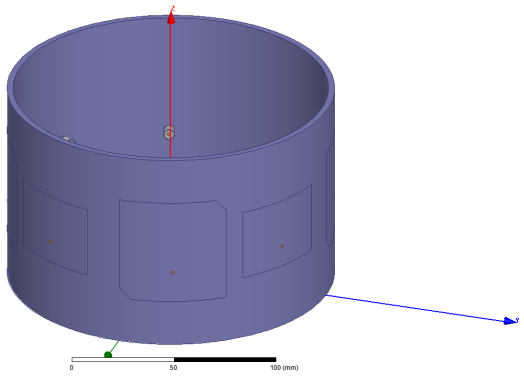

Fig. 3.59: Two types of antenna arrays without the booms.

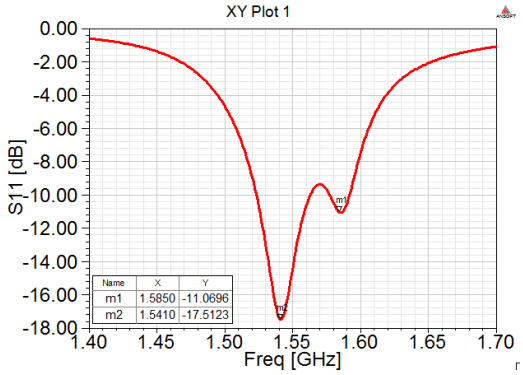

Fig. 3.60: S11 of the CPd GPS antenna.

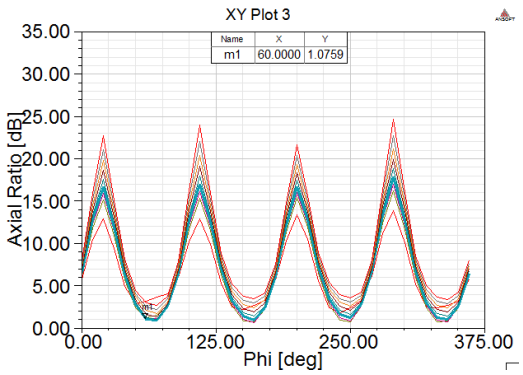

Fig. 3.61: AR, from 1.578 - 1.589 GHz.

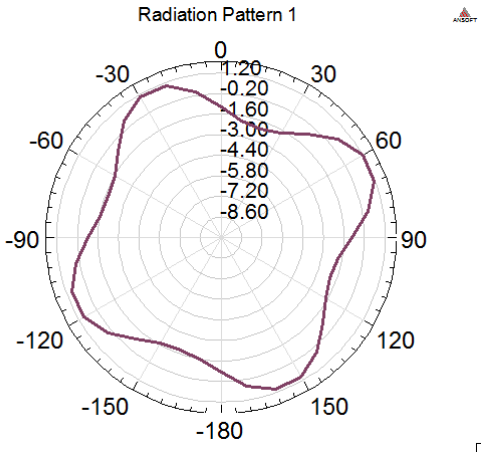

Fig. 3.62: H-plane, boresight.

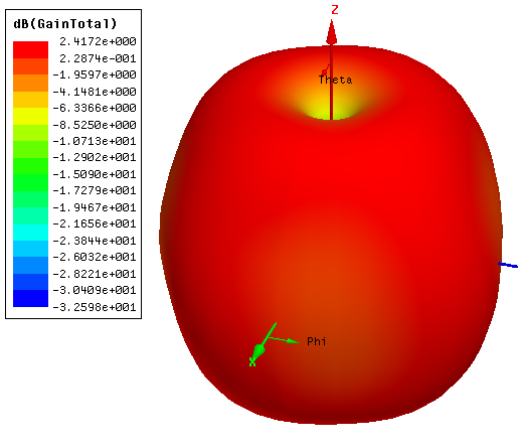

Fig. 3.63: 3-D radiation pattern.

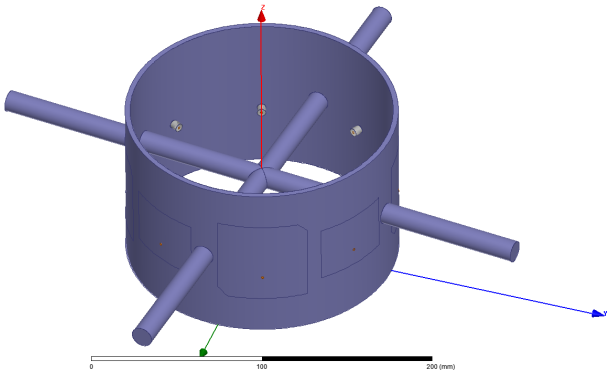

Fig. 3.64: Two typed of antenna arrays with the short booms.

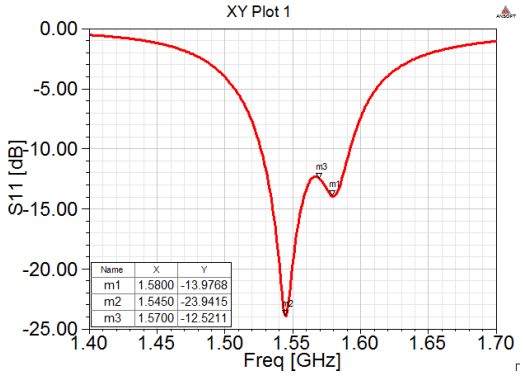

Fig. 3.65: S11 of the CPd GPS antenna.

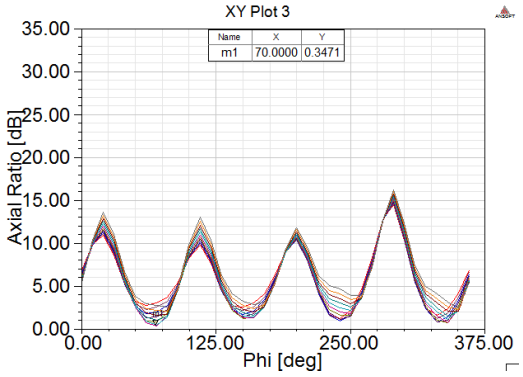

Fig. 3.66: AR, from 1.565 - 1.575 GHz.

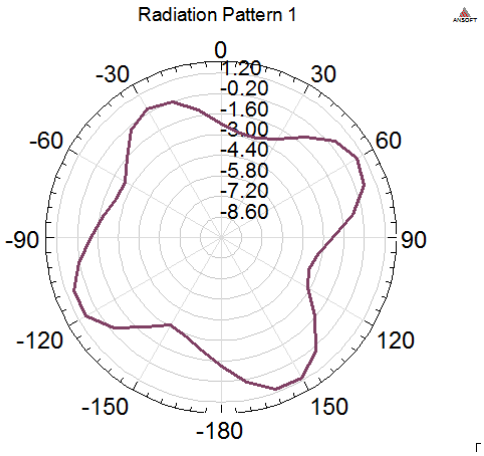

Fig. 3.67: H-plane, boresight.

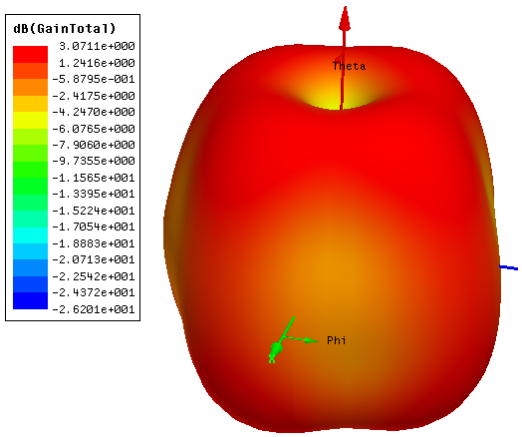

Fig. 3.68: 3-D radiation pattern.

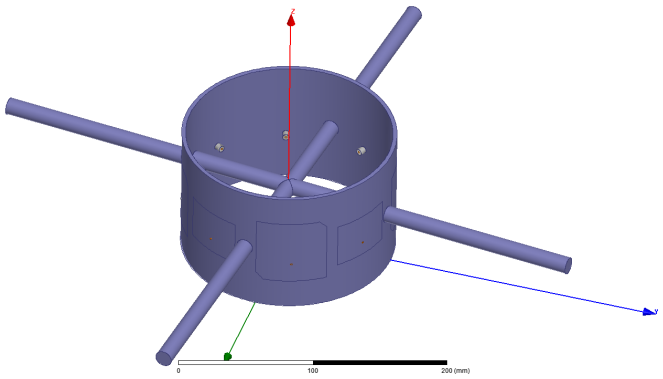

Fig. 3.69: Two types of antenna arrays with longer booms.

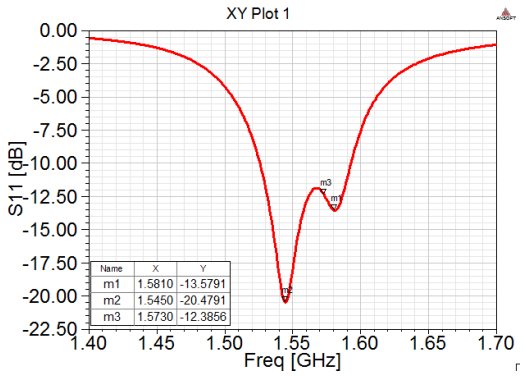

Fig. 3.70: S11 of the CPd GPS antenna.

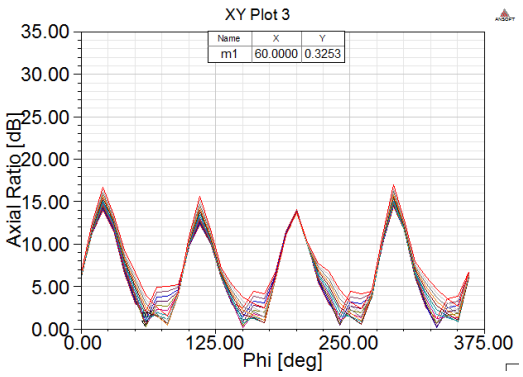

Fig. 3.71: AR, from 1.569 - 1.583 GHz.

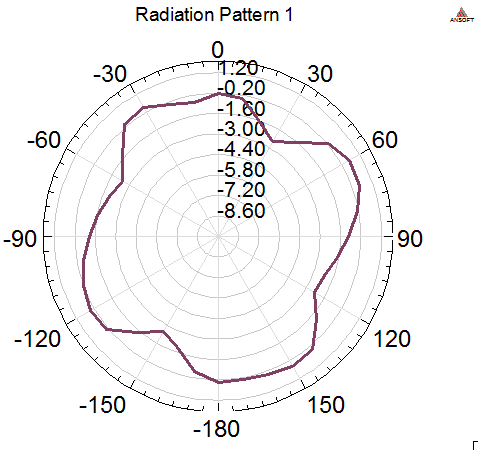

Fig. 3.72: H-plane, boresight.

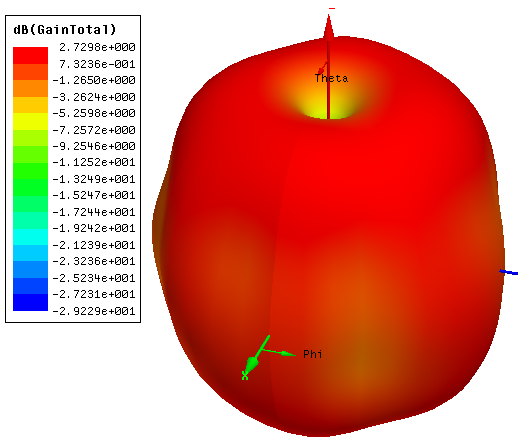

Fig. 3.73: 3-D radiation pattern.

to expect cross signal contamination, which is the bad isolation between the S band and GPS antenna signals. In order to see how bad the isolation could be, an HFSS simulation was performed as shown in Fig. 3.74. Its isolation plots are shown in Figs. 3.75-3.76. The isolation value was obtained by exciting one type of antenna while terminating the other. As expected, the isolation value between the two antennas was found to be around -20 dB, which is far away from the required -40 dB of isolation. One method of decreasing the isolation level is to increase the size of the cylinder so that the patches can be separated further. However, even though the size of the cylinder was increased to twice that of the original one, as shown in Fig. 3.77, the -40 dB isolation still could not be obtained (Figs. 3.78-3.79). This suggest the size of the cylinder should be further enlarged. Because there is not much freedom of increasing the size, using a notch filter or a band pass filter was proposed as a solution for the isolation problem.

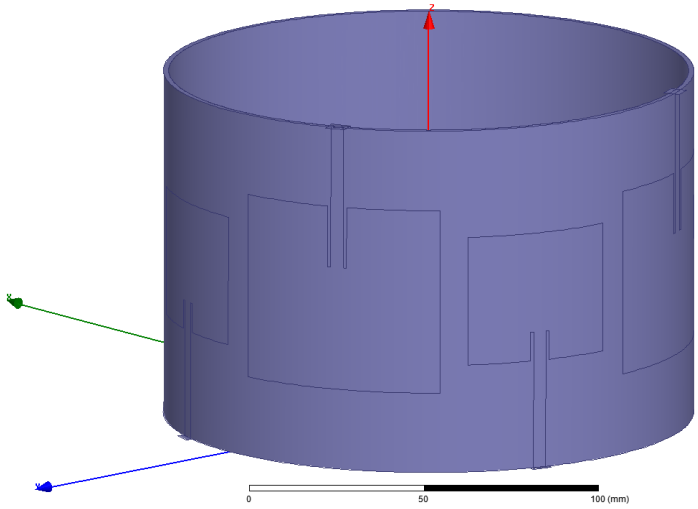

Fig. 3.74: Cylindrical structure with the original size.

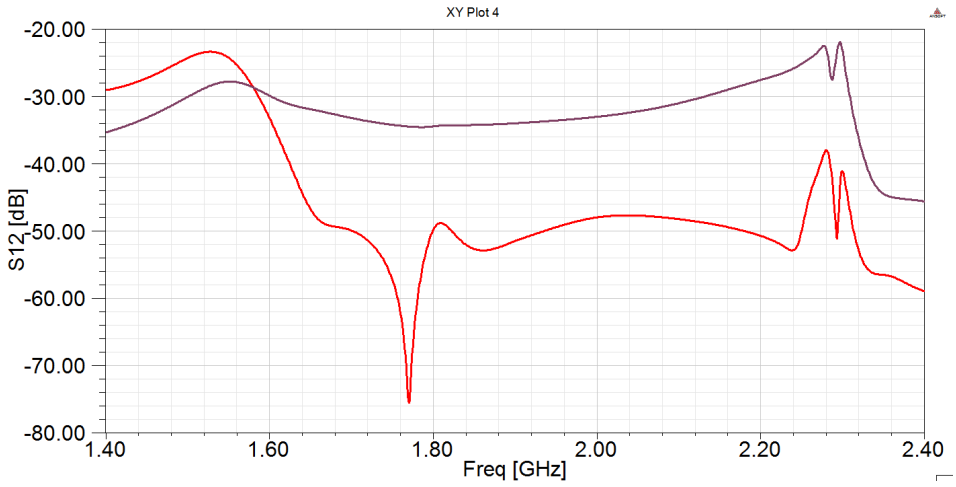

Fig. 3.75: S12 of the original cylindrical structure (GPS exited, S-band terminated).

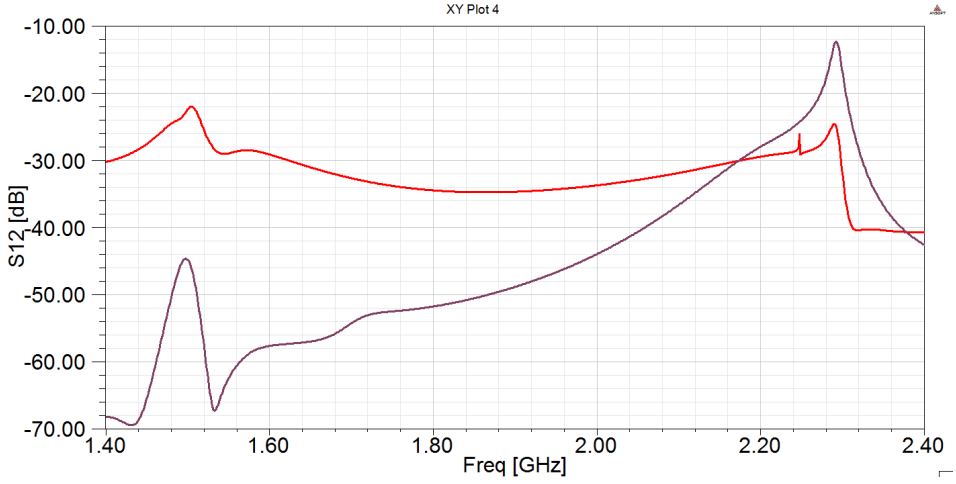

Fig. 3.76: S12 of the original cylindrical structure (S-band exited, GPS terminated).

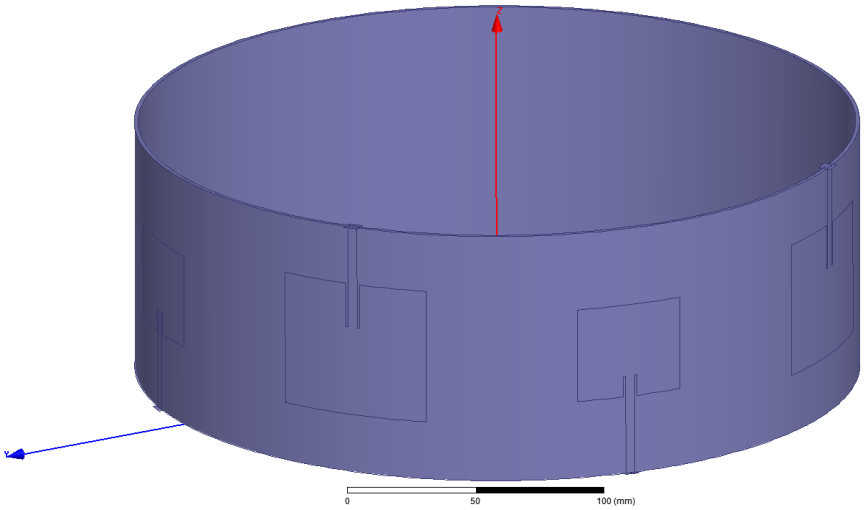

Fig. 3.77: Cylindrical structure with twice of the original size.

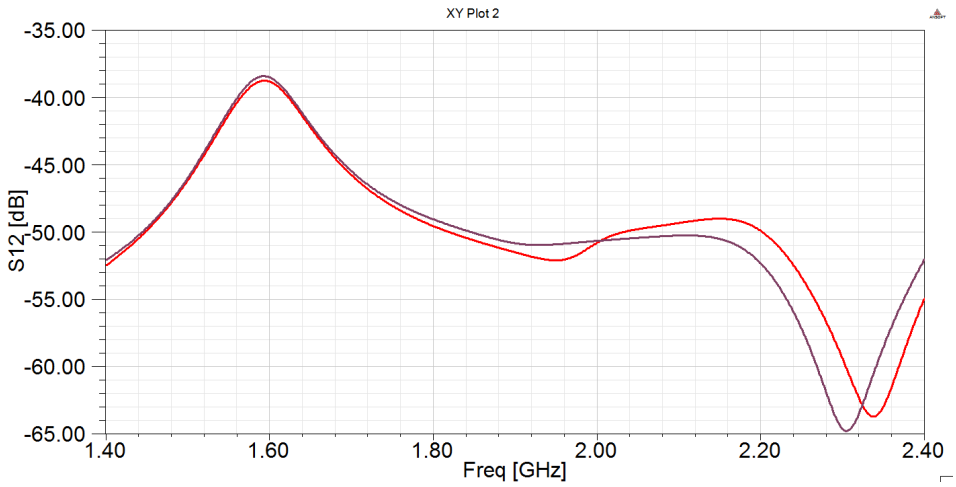

Fig. 3.78: S12 of the enlarged cylindrical structure (GPS exited, S-band terminated).

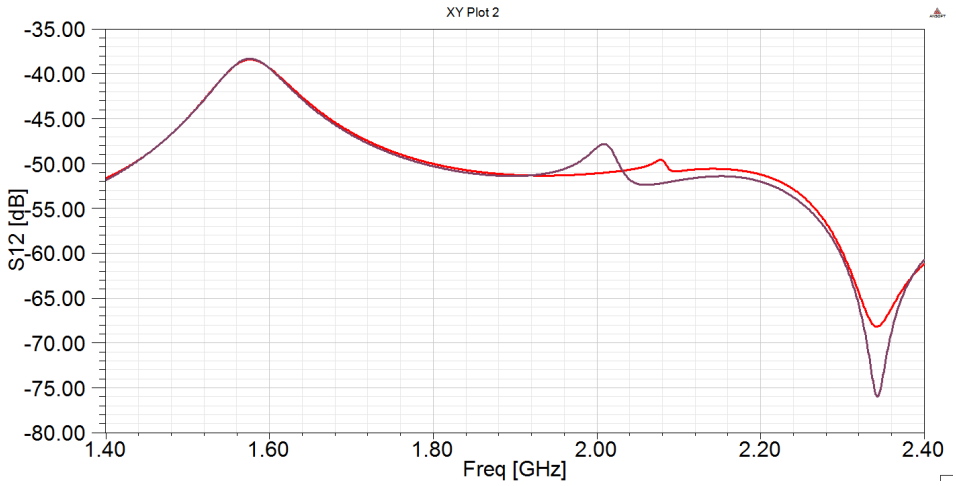

Fig. 3.79: S12 of the enlarged cylindrical structure (S-band exited, GPS terminated).

Chapter 4

Summary and Future Work

As the first phase of this research work, an inexpensive inkjet printing method was developed for fast, low-cost fabrication of electronic devices. Its reliability was verified through prototyping and testing LPd and CPd planar and conformal microstrip antennas. Comparison of the measurement results of the printed microstrip antenna with those of the copper microstrip antennas demonstrates that the printing method is quite reliable in validating HFSS antenna design. The printed antenna's efficiency was observed to be lower than the copper antenna, and the cause of the problem was addressed through analyzing the effect of the conductive ink's conductivity and thickness on the radiation efficiency of the printed antenna. For future work, the proposed inkjet printing method can be applied in other types of microwave device fabrication such as coplanar waveguide, RFID, and other types of 2-D passive antennas. In order to increase the resolution, relatively advanced inkjet printers can be used to find a trade-off between printing quality and cost of printing. The efficiency of printed antennas, however, can only be improved through developing better conductive ink that has higher conductivity.

In the second phase of this research work, the sub-payload antenna design was introduced in detail. Various challenges such as avoiding feed line interference, improving the isolation, characterizing the boom effect, and designing LPd conformal S-band antenna array and CPd conformal GPS antenna array, were confronted in the design process. A multilayer antenna structure was proposed as a solution to the feed line interference problem; using a notch filter or a band pass filter was suggested as a possible way of obtaining the required -40 dB of isolation; the possible effects of the booms were investigated through theoretical reasoning and extensive HFSS simulation, and reliable S-band and GPS conformal antenna arrays were designed with and without including the booms. The inkjet

printing method was conveniently applied in validating some of the antenna designs. For future work, further simulations can be carried out on the multilayer antenna structure. In the end, the S-band and GPS antenna arrays with the actual booms can be fabricated and tested in order to validate the HFSS simulation results.

References

[1] E. Tekin, P. J. Smith, and U. S. Schubert, "Inkjet printing as a deposition and patterning tool for polymers and inorganic particles," *Soft Matter*, vol. 4, pp. 703–713, 2008. [Online]. Available: http://dx.doi.org/10.1039/B711984D

[2] S. P. Speakman, G. G. Rozenberg, K. J. Clay, W. I. Milne, A. Ille, I. A. Gardner, E. Bresler, and J. H. Steinke, "High performance organic semiconducting thin films: Inkjet printed polythiophene [rr-p3ht]," *Organic Electronics*, vol. 2, no. 2, pp. 65–73, 2001. [Online]. Available: http://www.sciencedirect.com/science/article/pii/S1566119901000118

[3] D. Hayes, M. Grove, and W. Cox, "Development and application by inkjet printing of advanced packaging materials," *Advanced Packaging Materials: Processes, Properties and Interfaces. Proceedings. International Symposium*, pp. 88–93, March 1999.

[4] O. Azucena, J. Kubby, D. Scarbrough, and C. Goldsmith, "Inkjet printing of passive microwave circuitry," *Microwave Symposium Digest, 2008 IEEE MTT-S International*, pp. 1075–1078, June 2008.

[5] D. Redinger, S. Molesa, S. Yin, R. Farschi, and V. Subramanian, "An inkjet-deposited passive component process for RFID," *IEEE Transactions on Electron Devices*, vol. 51, no. 12, pp. 1978–1983, 2004. [Online]. Available: http://ieeexplore.ieee.org/xpls/abs_all.jsp?arnumber=1362956

[6] L. Yang, A. Rida, R. Vyas, and M. Tentzeris, "RFID tag and RF structures on a paper substrate using inkjet-printing technology," *IEEE Transactions on Microwave Theory and Techniques*, vol. 55, no. 12, pp. 2894–2901, 2007. [Online]. Available: http://ieeexplore.ieee.org/xpls/abs_all.jsp?arnumber=4383080

[7] A. Rida, L. Yang, R. Vyas, and M. Tentzeris, "Conductive inkjet-printed antennas on flexible low-cost paper-based substrates for RFID and WSN applications," *IEEE Antennas and Propagation Magazine*, vol. 51, no. 3, pp. 13–23, June 2009.

[8] G. Shaker, S. Safavi-Naeini, N. Sangary, and M. Tentzeris, "Inkjet printing of ultra-wideband (UWB) antennas on paper-based substrates," *IEEE Antennas and Wireless Propagation Letters*, vol. 10, pp. 111–114, 2011.

[9] J. A. Arellano, "Inkjet-printed highly transparent solar cell antennas," Master's thesis, Utah State University, Logan, 2011.

[10] F. Boeykens, L. Vallozzi, and H. Rogier, "Cylindrical bending of deformable textile rectangular patch antennas," *International Journal of Antennas and Propagation*, vol. 2012, 2012.

[11] H.-M. Chen, Y.-K. Wang, Y.-F. Lin, C.-Y. Lin, and S.-C. Pan, "Microstrip-fed circularly polarized square-ring patch antenna for GPS applications," *IEEE Transactions on Antennas and Propagation*, vol. 57, no. 4, pp. 1264–1267, 2009. [Online]. Available: http://ieeexplore.ieee.org/xpls/abs_all.jsp?arnumber=4812209

[12] C. Balanis, *Antenna theory: analysis and design*. New York: John Wiley and Sons, 1982.

[13] P. C. Sharma and K. C. Gupta, "Analysis and optimized design of single feed circularly polarized microstrip antennas," *IEEE Transactions on Antennas and Propagation*, vol. 31, pp. 949–955, Nov. 1983.

[14] T. Kellomäki, "Analysis of circular polarization of cylindrically bent microstrip antennas," *International Journal of Antennas and Propagation*, vol. 2012, 2012. [Online]. Available: http://www.hindawi.com/journals/ijap/2012/858031/abs/

[15] N. Padros, J. I. Ortigosa, J. Baker, M. F. Iskander, and B. Thornberg, "Comparative study of high-performance GPS receiving antenna designs," *IEEE Transactions on Antennas and Propagation*, vol. 45, no. 4, pp. 698–706, 1997. [Online]. Available: http://ieeexplore.ieee.org/xpls/abs_all.jsp?arnumber=564096

[16] T. Kellomaki, J. Heikkinen, and M. Kivikoski, "Effects of bending GPS antennas," *Microwave. Proceedings. 2006 IEEE Asia-Pacific Microwave Conference*, pp. 1597–1600, 2006. [Online]. Available: http://ieeexplore.ieee.org/xpls/abs_all.jsp?arnumber=4429712

[17] X. Quan, R. Li, and M. Tentzeris, "A novel broadband omni-directional circularly polarized antenna for mobile communications," *Antennas and Propagation (APSURSI), 2011 IEEE International Symposium*, pp. 1777–1779, July 2011.

[18] K. Sakaguchi and N. Hasebe, "A circularly polarized omnidirectional small helical antenna," *Antennas and Propagation, Ninth International Conference (Conference Publication No. 407)*, vol. 1, pp. 492–495, April 1995.

[19] L. Zong-quan, Q. Zu-ping, H. Zhen-ping, and N. Wei-min, "Design of a circularly polarized conformal microstrip antenna with CPW-fed," *Electronics, Communications and Control (ICECC), International Conference*, pp. 206–209, Sept. 2011.

[20] R. Pant, P. Kala, S. Pattnaik, and R. Saraswat, "A circularly polarized rectangular patch antenna on a cylindrical surface," *International Journal of Microwave and Optical Technology*, pp. 443–444, 2008.

[21] K. Wong and S. Ke, "Cylindrical-rectangular microstrip patch antenna for circular polarization," *IEEE Transactions on Antennas and Propagation*, vol. 41, no. 2, pp. 246–249, 1993. [Online]. Available: http://ieeexplore.ieee.org/xpls/abs_all.jsp?arnumber=214621